

Optimal Representation of the Density Field
from Redshift Surveys

by

Elke Schumacher

Thesis
submitted to the
University of Glasgow
for the degree of
Master of Science

Astronomy and Astrophysics Group
Department of Physics and Astronomy
University of Glasgow
G12 8QQ

August 2000

ProQuest Number: 13833940

All rights reserved

INFORMATION TO ALL USERS

The quality of this reproduction is dependent upon the quality of the copy submitted.

In the unlikely event that the author did not send a complete manuscript and there are missing pages, these will be noted. Also, if material had to be removed, a note will indicate the deletion.



ProQuest 13833940

Published by ProQuest LLC (2019). Copyright of the Dissertation is held by the Author.

All rights reserved.

This work is protected against unauthorized copying under Title 17, United States Code
Microform Edition © ProQuest LLC.

ProQuest LLC.
789 East Eisenhower Parkway
P.O. Box 1346
Ann Arbor, MI 48106 – 1346

GLASGOW
UNIVERSITY
LIBRARY

12068-Cop 1

Abstract

This thesis presents a method to reconstruct the density field in the local universe from flux limited nearly all-sky redshift surveys. As a first application we reconstruct the overdensity field in redshift space up to redshifts of $20,000 \text{ km s}^{-1}$ from the PSCz catalogue of [Saunders et al. 2000].

One of the most important issues that needs to be considered for this task is the impact of selection effects. So far no redshift catalogue contains all existing galaxies (up to a certain distance) but a subset that is chosen according to certain selection criteria. Usually the region close to the galactic plane is not observed because it is obscured by the Milky Way, and as the distance increases, more and more galaxies become too faint to be detected, so that at large distances only very luminous galaxies are included in the catalogue. The former selection criterion can be expressed as an angular mask, and the latter is described by the selection function, which can be interpreted as a radial mask.

Due to the spherical symmetry of nearly all-sky redshift surveys it is an obvious choice to expand the density (and also the velocity and potential) field using Spherical Harmonics and Spherical Bessel Functions, which are a set of orthonormal basis functions on a completely observed spherical volume. This basis also allows a separation of angular and radial effects, e.g. the distortion due to the peculiar motions, which affects only the radial component.

The calculation is complicated by the existence of the angular mask and the selection function. The difficulties arise because the volume is not observed completely, and these basis functions lose their orthogonality. Thus expansion coefficients are not independent.

Therefore we construct a new set of basis functions that are orthonormal on the angular and radial masked space. They are linear combinations of the Spherical Harmonics and Spherical Bessel Functions. The method is an extension to three dimensions of the orthonormalisation procedure of [Gorski 1994]. Due to the orthonormality the expansion coefficients of this basis can be computed independently and for any error analysis they can also be treated as statistically independent, which are both useful properties. The linear relation allows us to transform between the coefficients of the two bases.

First of all we need to determine the selection function of the redshift catalogue. Therefore we apply a robust method that is related to the C^- -Method of [Lynden-Bell 1971]. This method assumes a universal luminosity function, but makes no assumption about the spatial distribution of the galaxies or the parametric form of the luminosity function. Tests on mock catalogues yield an error in the selection function of 14% up to redshifts of $30,000 \text{ km s}^{-1}$. The comparison of the derived selection function with the data of the PSCz catalogue shows a good agreement in the range of these uncertainties up to redshifts of $20,000 \text{ km s}^{-1}$.

We reconstruct the overdensity field in redshift space up to redshifts of $20,000 \text{ km s}^{-1}$. The procedure involves the inversion of a large matrix, hence we invert the matrix via Singular Value Decomposition and apply a linear regularisation method.

We tested the influence of the choice of the maximum redshift and of the truncation in the expansion series and did not find the results sensitive to them. We also replaced our selection function with the one of [Saunders et al. 2000], but only the amplitude of the density peaks was slightly affected.

We find our reconstructed overdensity field in a good agreement with the data, and also with other recent results.

In the final chapter we outline how the derived redshift space density field can be transformed to real space and how the results can be applied e.g. for power spectrum estimation.

Contents

1	Introduction	10
1.1	Evolution of Large Scale Structure	11
1.1.1	Self-Gravitating Collisional Gas in a Static Universe	11
1.1.2	Matter-Dominated Expanding Universe	14
1.1.3	Radiation-Dominated Expanding Universe	15
1.1.4	The Zel'dovich Approximation	16
1.2	Power Spectrum	17
1.3	Observational Data	18
1.4	Goal	19
2	The Method	20
2.1	Some Background Details	21
2.1.1	Selection Function and Luminosity Function	21
2.1.2	Smoothing Procedure	21
2.1.3	Expansion in Orthonormal Functions	22
2.1.4	The Mask	22
2.1.5	Shot Noise	23
2.1.6	A Short Outline of our Method	24
2.2	Reconstructing the Selection Function	25
2.2.1	K-Correction	26
2.2.2	Luminosity Function	27
2.3	Expanding the Density Field	30
2.3.1	Spherical Harmonics and Spherical Bessel Functions	30
2.3.2	Problems due to the Mask and the Selection Function	31
2.3.3	Dealing with the Mask and the Selection Function	32
2.4	Singular Value Decomposition (SVD)	34

<i>CONTENTS</i>	4
2.5 Linear Regularisation	36
2.6 The Method summarised	37
3 Applying the Method to Data, Tests	39
3.1 Finding the Selection Function	42
3.1.1 Tests on Mock Catalogues	42
3.2 Applying the Expansion	44
3.2.1 Finding l_{max} and n_{max}	44
3.2.2 Choice of Boundary Condition	48
3.2.3 Computing the Matrix Elements W_{ij}	49
3.3 Applying SVD	49
3.4 Computation of Coefficients by Linear Regularisation, Error Estimation	51
3.5 The Applied Procedure summarised	54
4 Results and Discussion	56
4.1 Selection Function	56
4.2 A Cosmographical Tour	58
4.2.1 Behind the Mask	63
4.2.2 Discussion	64
5 Conclusions	71
5.1 Future Work	72
5.1.1 Going to Real Space	72
5.1.2 Power Spectrum Estimation	73
List of References	75

List of Figures

2.1	Illustration of the SF-Method	29
3.1	PSCz Galaxies and Mask	40
3.2	$n(r_s)$ -Plot	41
3.3	Tests of Reconstructing the Selection Function	45
3.4	Singular Value Spectrum	50
4.1	Reconstructed CLF	57
4.2	Selection Function and Comparison to Saunders' Result	57
4.3	Density Field in SGP, reconstructed with $V_{max} = 20,000\text{kms}^{-1}$	59
4.4	Reconstructed Density Field in Shells	60
4.5	Density Field in SGP from [Fisher et al. 1995]	64
4.6	Density field in SGP, reconstructed with $V_{max} = 25,000\text{kms}^{-1}$	66
4.7	Density field in SGP, with Saunders-SF	67
4.8	Reconstructed Density Field in Shells; with Saunders-SF	68
4.9	Errors in the reconstructed density field	70

Acknowledgements

Although I composed this thesis and did the majority of this work myself, many more people contributed to the completion of this thesis.

My first and greatest thanks go to my supervisor Dr. Martin Hendry. Although he is ever busy with thousands of things, he always found time to listen to my many questions and discuss and answer them. His enthusiasm for science and research can be really infectious!

Dr. Stephane Rauzy often joined our discussions, and whenever I knocked at his door with big question marks in my eyes he came and helped to sort out my confusion. Thanks a lot for that!

Dr. Stephane Rauzy and Dr. Martin Hendry provided the theory for the construction method for the luminosity function.

Especially during the last months also Dr. Richard Barrett joined our meetings. He guided me into the world of inverse theory. Thanks for helping to “diagnose” and “cure” my inverse problem!

Dr. Graeme Stewart and Dr. Norman Gray gave me a little insight in these miraculous machines called computers, which was of course very useful if you need to work with them every day. Thanks for that, and I’m sorry I crashed Phobos.

Special thanks go to Gail Penny and Helen Bryce with whom I shared an office during the last year. It was very kind of you to give me lifts to the airport and to invite me to some walks in this great country, Gail. And thanks for pushing me to run the 10K, which I never believed I would do until I reached the finish. Thanks to Helen I was always well informed about the latest pop news, and besides that her cheerfulness was very refreshing.

A special thank you goes to Helen and Richard for spending a weekend on the final check of this thesis.

Whenever I had a question not concerning physics or astronomy but bureaucracy and organising, Ms. Daphne Davidson could always help. A big thank-you for that, for it made life much easier.

Also thanks to all the other members of the Astro Group for small talk during coffee time, for parties, and for the warm welcome in this “family”. Good luck and success to all of you who intend to submit a thesis in the future!

There are some people outside the department who played an important role during the last year.

I want to thank Maria for being such a nice flatmate. I hope you’ll forgive me for blocking the phone so often. And thanks for the merry evenings, for which also Bessie and Teresa contributed a lot.

The members of the “Virtual Aikido Club” which are Anja, Antje, Carsten, Ole, Oliver, and Suse deserve warm thanks, and also Ingo, Jan, Anne, Sabine . . .; it is great how close you kept in touch with me throughout the whole year, when I’ll come back it will not feel as if I’ve ever been away.

There are so many things I want to say thank you for to my boyfriend Carsten. Thank you for sharing with me joy, dreams, and also fears, thanks for the long hours of talking, for the great ideas, the encouragement and all the love and patience. You make coming home an offer that I simply cannot refuse!

I can’t believe how quickly my little sister grew up, now she can even give counsel and comfort to me! Thank you a lot for that. I wish you good luck for your own studies, for two more years at school and then at a university, if you like.

I would never have got to where I am today if there had not been the constant support and love of my parents. They supported every particular interest I developed, even my decision to study something unusual as physics, and even astronomy. They constantly care about my well-being in every way. Although I did not visit you as often as I should have, you are giving me the feeling that there is a place where I can come home, even if the rest of the world ends.

Finally I wish to thank the German Academic Exchange Service (DAAD) for providing an important share of the financial support to make this year possible.

All these people have made this last year unforgettable. I have learned an incredible lot of things, many of them I did not expect to learn now and here. When I will have to say good bye I will do this with a laughing and a crying eye. I am looking forward to be home again, but I know I will miss the friendly people in Glasgow.

To my Parents

Abbreviations

CLF	Cumulative Luminosity Function
LF	Luminosity Function
MS	angular and radial Masked Space
SED	Spectral Energy Distribution
SB	Spherical Bessel Function
SF	Selection Function
SGP	SuperGalactic Plane
SH	Spherical Harmonics
SVD	Singular Value Decomposition

Chapter 1

Introduction

Let us bind together
Heaven and Earth, Kami and Man.
So we may guard and protect
This age of ours.

Morihei Ueshiba

Man has always been attempting to understand our environment, from the immediate surroundings to the world as a whole. This thesis belongs in the field of cosmology, which is the science that investigates the features and history of our universe.

Two of the most important assumptions in exploring the universe and its evolution are the Cosmological Principle which states that the universe looks approximately the same everywhere; and the Copernican Principle stating that humans are not privileged observers. Another way to express these principles is to say that the universe is isotropic and homogeneous. Of course this is an approximation, certainly at small scales but it is believed to improve at larger scales. However, if we look at our local neighbourhood we can see complex structures like stars and planets, galaxies, groups of galaxies, clusters, and superclusters, which are clearly not isotropic or homogeneous.

According to the widely accepted standard theory these structures grew by self-gravitation out of small fluctuations in a homogeneous density field. This process is called gravitational instability. The theory is strongly supported by the results of the COBE satellite which explored the cosmic microwave background (CMB). The measurements showed that the CMB was nearly perfectly isotropic, but with very small fluctuations in temperature depending on direction. These fluctuations indicate density perturbations in the primordial density field. However there are different theories which explain the origin of these small primordial

fluctuations, e.g. inflation and string theory.

One of the aims of contemporary research in cosmology is to measure the (local) density field and to explain its features and history.

1.1 Evolution of Large Scale Structure

There are excellent explanations of the evolution of large scale structure in e.g. [Coles 1997], [Coles and Lucchin 1995], and [Peacock 1999], so here we will give only a summary of this topic.

The evolution of density fluctuations is often described in terms of the overdensity or density contrast δ

$$\delta(\vec{x}, t) = \frac{\rho(\vec{x}, t) - \langle \rho \rangle}{\langle \rho \rangle}, \quad (1.1)$$

where $\langle \rho \rangle$ is the mean density. Structure formation on smaller scales is, in addition to gravity, also strongly influenced by e.g. star formation, shock waves, and supernova-feedback, so it is highly nonlinear, which is difficult to handle analytically. The large scale structure can be described, however in the linear or mildly nonlinear regime.

The growth of structure from primordial fluctuations in the mass density is a balance between the forces of gravitation and pressure. If a fluctuation is too small, or contains too little mass, it will vanish in time. If it is large enough, gravitation will “win” and the fluctuation will collapse. Jeans was the first to study such processes in detail, so the critical length and mass scales are called the Jeans length λ_J and Jeans mass m_J .

There are two different approaches to this topic: one can investigate perturbations in the density field, or particle displacements, which means following the trajectories of single particles. First we will explain the former method and start with the idealised case of a static universe filled with a collisional, self-gravitating gas. Then we will turn to an expanding matter- or radiation-dominated universe. The Newtonian approach yields the same results as the relativistic one, so we will use the former, because it is easier to handle. We will also explain the Zel’dovich approximation, which is a linear approximation with respect to particle displacements and so follows the second approach.

1.1.1 Self-Gravitating Collisional Gas in a Static Universe

The evolution of such a fluid is governed by the continuity equation describing the conservation of matter, the Eulerian equation, which describes the conservation of momentum, and

the Poisson equation, which expresses the influence of gravitation. Because we will neglect viscosity and thermal conductivity, we have to add the conservation of entropy per unit mass s . These are eqns. 1.2 to 1.5 respectively:

$$\frac{\partial \rho}{\partial t} + \nabla \cdot \rho \vec{v} = 0 \quad (1.2)$$

$$\frac{\partial \vec{v}}{\partial t} + (\vec{v} \cdot \nabla) \vec{v} + \frac{1}{\rho} \nabla p + \nabla \phi = 0 \quad (1.3)$$

$$\nabla^2 \phi - 4\pi G \rho = 0 \quad (1.4)$$

$$\frac{\partial s}{\partial t} + \vec{v} \cdot \nabla s = 0 \quad (1.5)$$

There exists a static solution with $\rho = \rho_0$ for the mass density, $v = 0$ for the velocity field, $s = s_0$ for the entropy per unit mass, $p = p_0$ for the pressure, and $\nabla \phi = 0$ for the gravitational potential. This solution has the problem that $\rho_0 \neq 0$ is not possible, because then the gravitational potential must vary spatially, or ρ must be either contracting or expanding. We ignore this problem at this stage and look for solutions for small perturbations of this static solution $\rho = \rho_0 + \delta\rho$, $\vec{v} = \delta\vec{v}$, $p = p_0 + \delta p$, $s = s_0 + \delta s$, $\phi = \phi_0 + \delta\phi$. Applying eqns. 1.2 to 1.5 to these perturbations and neglecting terms of second and higher order one obtains

$$\frac{\partial \delta\rho}{\partial t} + \rho_0 \nabla \cdot \delta\vec{v} = 0 \quad (1.6)$$

$$\frac{\partial \delta\vec{v}}{\partial t} + \frac{1}{\rho_0} \left(\frac{\partial p}{\partial \rho} \right)_s \nabla \delta\rho + \frac{1}{\rho_0} \left(\frac{\partial p}{\partial s} \right)_p \nabla \delta s + \nabla \delta\phi = 0 \quad (1.7)$$

$$\nabla^2 \delta\phi - 4\pi G \delta\rho = 0 \quad (1.8)$$

$$\frac{\partial \delta s}{\partial t} = 0 \quad (1.9)$$

These eqns. can be solved by plane waves, where \vec{k} is the (real) wave vector with $\lambda = 2\pi/k$, and ω is the frequency, which is in general complex:

$$\delta\rho = \delta_0 \rho_0 \exp(i\omega t) \exp(i\vec{k} \cdot \vec{r}) \quad (1.10)$$

$$\delta\vec{v} = \vec{V} \exp(i\omega t) \exp(i\vec{k} \cdot \vec{r}) \quad (1.11)$$

$$\delta\phi = \Phi \exp(i\omega t) \exp(i\vec{k} \cdot \vec{r}) \quad (1.12)$$

$$\delta s = \Sigma \exp(i\omega t) \exp(i\vec{k} \cdot \vec{r}) \quad (1.13)$$

So only the amplitudes need to be found. One can introduce the sound speed $v_s^2 = (\partial p / \partial \rho)_s$ and obtain the system of equations for the amplitudes:

$$\omega \delta_0 + \vec{k} \cdot \vec{V} = 0 \quad (1.14)$$

$$\omega \vec{V} + \vec{k} v_s^2 \delta_0 + \frac{\vec{k}}{\rho_0} \left(\frac{\partial \rho}{\partial s} \right)_s \Sigma + \vec{k} \Phi = 0 \quad (1.15)$$

$$k^2 \Phi + 4\pi G \rho_0 \delta_0 = 0 \quad (1.16)$$

$$\omega \Sigma = 0 \quad (1.17)$$

There are two major groups of solutions for these equations. In the first instance there are solutions with $\omega = 0$, implying $\vec{k}\vec{V} = 0$ and a free choice of Σ . The solution with $\Sigma \neq 0$ is called the entropic solution. If we choose $\Sigma = 0$, eqn. 1.16 and 1.17 show that there are no perturbations to the density in this case. As all the solutions with $\omega = 0$ are time independent anyway they are not important for the evolution of density perturbations.

Secondly there are solutions with $\omega \neq 0$, implying $\Sigma = 0$ and $\vec{k}\vec{V} \neq 0$; these are the more interesting time-dependent solutions. Because $\Sigma = 0$ there will be no fluctuations in entropy, the perturbations are adiabatic. As $\vec{k}\vec{V} \neq 0$, we can split the solution into one mode with $\vec{k} \perp \vec{V}$ (vortical mode) and one with $\vec{k} \parallel \vec{V}$ (longitudinal mode). For the vortical mode we have $\vec{k}\vec{V} = 0$ and $\Sigma = 0$ as before in the time independent case, and again because of eqn. 1.16 and 1.17 there are no density perturbations for the vortical mode. So the only interesting solution is the adiabatic longitudinal mode. In this case the system of equations for the amplitudes reduces to

$$\omega\delta_0 + kV = 0 \quad (1.18)$$

$$\omega V + kv_s^2\delta_0 + k\Phi = 0 \quad (1.19)$$

$$k^2\Phi + 4\pi G\rho_0\delta_0 = 0 \quad (1.20)$$

This has a non-zero solution if and only if the determinant equals zero, which gives the dispersion relation of these waves:

$$\omega^2 - v_s^2k^2 + 4\pi G\rho_0 = 0 \quad (1.21)$$

Using the definition of the Jeans wavelength

$$\lambda_J = v_s \left(\frac{\pi}{G\rho_0} \right)^{1/2} \quad (1.22)$$

one can distinguish two cases: In the first one with $\lambda < \lambda_J$ one obtains the real frequency

$$\omega = \pm v_s k \left[1 - \left(\frac{\lambda}{\lambda_0} \right)^2 \right]^{1/2} \quad (1.23)$$

which means that the density fluctuation is

$$\delta = \frac{\delta\rho}{\rho_0} = \delta_0 \exp[i(\vec{k} \cdot \vec{r} \pm |\omega|t)]. \quad (1.24)$$

These are just two sound waves, no perturbations grow or decay.

In the case of $\lambda > \lambda_J$ the frequency is imaginary

$$\omega = \pm i(4\pi G\rho_0)^{1/2} \left[1 - \left(\frac{\lambda_J}{\lambda} \right)^2 \right]^{1/2} \quad (1.25)$$

and thus the density fluctuation is

$$\delta = \frac{\delta\rho}{\rho_0} = \delta_0 \exp(i\vec{k} \cdot \vec{r}) \exp(\pm|\omega|t). \quad (1.26)$$

This is a stationary wave with either increasing or decreasing amplitude. This is the only kind of solution that describes the phenomenon of gravitational instability.

1.1.2 Matter-Dominated Expanding Universe

For simplicity we only consider the case of dust, in which the pressure is zero. The following equations describe the expansion/contraction of a homogeneous and isotropic mass distribution, which is also a solution of eqns. 1.2 to 1.5:

$$\rho = \rho_0 \left(\frac{a_0}{a}\right)^3 \quad (1.27)$$

$$\vec{v} = \frac{\dot{a}}{a} \vec{r} \quad (\text{Hubble's law}) \quad (1.28)$$

$$\phi = \frac{2}{3} \pi G \rho r^2 \quad (1.29)$$

$$p = p(\rho, s) \quad (1.30)$$

$$s = \text{const.} \quad (1.31)$$

The vector \vec{r} is a physical distance, related to the comoving coordinate \vec{r}_0 by $\vec{r} = \frac{a}{a_0} \vec{r}_0$; a is the expansion factor at the time t and a_0 is the current value of the expansion factor. This solution also has a problem, which is that ϕ and v diverge for $r \rightarrow \infty$. It does not influence our calculations here, but it could be avoided in a relativistic treatment. We again perturb the homogeneous solution and find the equations for the perturbations, neglecting terms of second and higher order:

$$\dot{\delta\rho} + 3\frac{\dot{a}}{a}\delta\rho + \frac{\dot{a}}{a}(\vec{r} \cdot \nabla)\delta\rho + \rho(\nabla \cdot \delta\vec{v}) = 0 \quad (1.32)$$

$$\delta\vec{v} + \frac{\dot{a}}{a}\delta\vec{v} + \frac{\dot{a}}{a}(\vec{r} \cdot \nabla)\delta\vec{v} = -\frac{1}{\rho}\nabla p + \nabla\delta\phi \quad (1.33)$$

$$\nabla^2\delta\phi - 4\pi G\delta\rho = 0 \quad (1.34)$$

$$\dot{\delta s} + \frac{\dot{a}}{a}(\vec{r} \cdot \nabla)\delta s = 0 \quad (1.35)$$

The dots denote partial derivatives with respect to time.

Now we look for solutions $\delta u_i = u_i(t) \exp(i\vec{k}\vec{r})$, with $u_i = (D = \delta\rho), \vec{V}, \Phi, \Sigma$ for $i = 1, 2, 3, 4$. The $u_i(t)$ cannot be of the form $\exp(i\omega t)$ because the coefficients in this system of equation depend upon time.

Also the wavelength λ varies with time because of the expansion

$$k = \frac{2\pi}{\lambda} = \frac{2\pi}{\lambda_0} \frac{a_0}{a} = k_0 \frac{a_0}{a}. \quad (1.36)$$

As we have seen in the previous subsection, the only cosmologically interesting solution is obtained with $\Sigma = 0$ and $\vec{V} \parallel \vec{k}$. This gives a differential equation for δ :

$$\ddot{\delta} + 2\frac{\dot{a}}{a}\dot{\delta} + (v_s^2 k^2 - 4\pi G\rho)\delta = 0 \quad (1.37)$$

To solve for δ we need to specify the cosmological model. For example, for a flat, matter-dominated Einstein-de Sitter universe with monoatomic particles of mass m , which is characterised by

$$\rho = \frac{1}{6\pi G t^2}, \quad a = a_0 \left(\frac{t}{t_0}\right)^{2/3}, \quad \frac{\dot{a}}{a} = \frac{2}{3t}, \quad (1.38)$$

one obtains

$$\ddot{\delta} + \frac{4}{3}\frac{\dot{\delta}}{t} - \frac{2}{3t^2}\left(1 - \frac{v_s^2 k^2}{4\pi G\rho}\right)\delta = 0. \quad (1.39)$$

This is easy to solve for $k \rightarrow 0$, that means large wavelengths: it has a growing solution $\delta_+ \propto t^{2/3}$ and a decaying solution $\delta_- \propto t^{-1}$. The Jeans wavelength is the same as in the previous case.

1.1.3 Radiation-Dominated Expanding Universe

In this case we have to consider radiation pressure, and for pure radiation the equation of state is $p = 1/3\rho c^2$. We also have to apply relativistic theory. Then the equations analogous to 1.2 to 1.5 become (see [Coles 1997])

$$\frac{\partial \rho}{\partial t} + \nabla \cdot \rho \vec{v} + \frac{p}{c^2} \nabla \cdot \vec{v} = 0 \quad (1.40)$$

$$\left(\rho + \frac{p}{c^2}\right) \left(\frac{\partial \vec{v}}{\partial t} + \vec{v} \cdot \nabla \vec{v}\right) + \nabla p + \left(\rho + \frac{p}{c^2}\right) \nabla \phi = 0 \quad (1.41)$$

$$\nabla^2 \phi - 4\pi G \left(\rho + 3\frac{p}{c^2}\right) = 0 \quad (1.42)$$

As we are only interested in adiabatic longitudinal modes, we do not need to include the entropic equation. Following the same procedure as before with $v_s = c/\sqrt{3}$ one obtains

$$\ddot{\delta} + 2\frac{\dot{a}}{a}\dot{\delta} + \left(v_s^2 k^2 - \frac{32}{3}\pi G\rho\right)\delta = 0. \quad (1.43)$$

In a flat radiation-dominated universe, which is characterised by

$$\rho = \frac{3}{32\pi G t^2}, \quad a = a_{eq} \left(\frac{t}{t_{eq}}\right)^{1/2}, \quad \frac{\dot{a}}{a} = \frac{1}{2t}, \quad (1.44)$$

the differential equation for the perturbation δ is reduced to

$$\ddot{\delta} + \frac{\dot{\delta}}{t} - \frac{1}{t^2}\left(1 - \frac{3v_s^2 k^2}{32\pi G\rho}\right)\delta = 0 \quad (1.45)$$

For $k \rightarrow 0$ one again finds a growing solution $\delta_+ \propto t$, and a decaying solution $\delta_- \propto t^{-1}$. For a radiation dominated universe, however, the Jeans wavelength is different:

$$\lambda'_J = v_s \left(\frac{3\pi}{8G\rho} \right)^{1/2} \quad (1.46)$$

1.1.4 The Zel'dovich Approximation

The previously outlined model was an Eulerian theory, describing the evolution of the density field. The Zel'dovich approximation is a Lagrangian theory, this means that it follows the trajectories of single particles, it is a linear approximation with respect to particle displacements. It begins with a uniformly distributed set of particles. Then each particle is displaced, this generates the density perturbation. The Lagrangian or initial coordinate of one particle is called \vec{q} , the Eulerian coordinate of this particle at time t is

$$\vec{r}(t, \vec{q}) = a(t)[\vec{q} - b(t)\nabla_q \Phi_0(\vec{q})] \quad (1.47)$$

The Eulerian coordinate \vec{r} is related to the comoving coordinate \vec{x} by $\vec{r} = a(t)\vec{x}$, $a(t)$ is the dimensionless expansion factor. The function $b(t)$ describes the evolution of a perturbation in the linear regime, so it is a solution of eqn. 1.37. For a flat matter-dominated universe we have $b \propto t^{2/3}$. The function $\Phi_0(\vec{q})$ is proportional to a velocity potential, which means that the flow is irrotational:

$$\vec{V} = \frac{d\vec{r}}{dt} - H\vec{r} = a \frac{d\vec{x}}{dt} = -ab\nabla_q \Phi_0(\vec{q}). \quad (1.48)$$

So in the linear regime the density perturbation and $\Phi_0(\vec{q})$ are related by

$$\delta = b\nabla_q^2 \Phi_0. \quad (1.49)$$

If the displacement is small, eqn. 1.47 defines a unique mapping between the coordinates \vec{r} and \vec{q} , so that

$$\rho(\vec{r}, t) = \frac{\langle \rho \rangle}{|J(\vec{r}, t)|} = \langle \rho \rangle \prod_{i=1}^3 [1 + b(t)\alpha_i(\vec{q})]^{-1} \quad (1.50)$$

$|J(\vec{r}, t)|$ is the Jacobian of the mapping. The matrix J is symmetric because the flow is irrotational, hence it can be diagonalised. The $[1 + b(t)\alpha_i]$ are the eigenvalues of J . In the linear regime we can approximate the last eqn. by

$$\delta \simeq -(\alpha_1 + \alpha_2 + \alpha_3)b(t). \quad (1.51)$$

Eqn. 1.50 expresses that the collapse of an overdense region will occur first along the axis defined by the most negative eigenvalue. This is exactly what you would expect if a perturbation is not perfectly spherical, then it should collapse into a flat structure, called a ‘‘pancake’’.

The Zel'dovich approximation works quite well up to the instance when two Lagrangian coordinates meet at the same Eulerian coordinate, this event is called a shell crossing, when this theory breaks down completely.

1.2 Power Spectrum

The power spectrum of the density fluctuation is a function that describes the “clumpiness” of the matter distribution in different length scales. One can expand the overdensity field in Fourier modes:

$$\delta(\vec{r}) = \frac{1}{(2\pi)^3} \int d^3k \tilde{\delta}(\vec{k}) e^{-i\vec{k}\vec{r}}, \quad (1.52)$$

where $\tilde{\delta}(\vec{k})$ is the Fourier transform of the overdensity.

The power spectrum $P(k)$ is defined as

$$\langle \tilde{\delta}(\vec{k}_1) \tilde{\delta}(\vec{k}_2) \rangle = (2\pi)^3 P(k_1) \delta_D(\vec{k}_1 - \vec{k}_2), \quad (1.53)$$

$\delta_D(\vec{r})$ is the Dirac-delta-function. The corresponding quantity in real space is the autocorrelation function

$$\zeta(r) = \langle \delta(\vec{x}) \delta(\vec{x} + \vec{r}) \rangle \quad (1.54)$$

which is the Fourier transform of the power spectrum. Since the universe is assumed to be isotropic, the autocorrelation function and the power spectrum may not depend on direction but only on the distance r or the length of the wave vector k . The $\tilde{\delta}(\vec{k})$ is a complex function, and a common assumption is that its phases are random. In this case the density is a Gaussian random field, which is predicted by the inflationary paradigm. The properties of random phases also mean that the power spectrum or the autocorrelation function is a complete statistical description of the density field, hence the power spectrum is an important quantity to characterise the density (or overdensity) field. One has to keep in mind that it is usually the distribution of the galaxies that is measured, and not the distribution of the mass. It is assumed that the galaxies trace the mass in a certain way, e.g. that the peaks in both density fields are the same. The quantity that relates the two distributions is called the bias parameter b , it can be defined e.g. in terms of the power spectrum:

$$P_{gal}(k) = b^2 P_{mass}(k) \quad (1.55)$$

We need to make a comment on the averages. In the statistical description of the evolution of the universe the averages should be ensemble averages. Since we can observe only our

unique universe, usually the Ergodicity Hypothesis is assumed. It states that the ensemble average and a volume average over a sufficiently large volume are the same and so gives an opportunity to compute the desired averages.

1.3 Observational Data

The outlined theory of the evolution of large scale structure always deals with the mass density. So far the only direct way to detect matter in the universe is to look for its radiation, so a way to measure the density is to build up galaxy catalogues containing the position of the galaxies and some more useful information such as their apparent magnitudes.

Unfortunately, detectors do often have a limiting sensitivity, which means that such catalogues usually contain only galaxies up to a certain limiting apparent magnitude (or flux). This behaviour can be expressed in terms of a selection function. A second problem arises: one would like to collect data from all over the sky, but our own galaxy covers a part of it, making measurements close to the galactic plane impossible or too noisy to be reliable; the catalogue will be “masked”.

The PSCz catalogue (Point Source Catalogue; z stands for redshift) provided by [Saunders et al. 2000] is one such catalogue, it contains 14677 galaxies with redshifts (and some more without). It is based on the data of the Infrared Astronomical Satellite (IRAS) which flew in 1983 and carried out a nearly full sky survey with a resolution of 1 arcminute. Flux measurements in 4 broad bands centred at 12, 25, 60, and $100\mu m$ were taken. Measurements in the IR have the advantage of being less affected by galactic extinction, but early-type galaxies contain little dust or have no star formation, so they are generally not present in the IRAS samples. To ensure that the catalogue contains only galaxies but not stars or nebulae certain relations between the fluxes in the different bands were required (for detail see [Saunders et al. 2000]). In addition to the “usual” galactic mask the PSCz mask covers two more narrow stripes and some isolated spots on the sky because the satellite ran out of cryostat before finishing the survey. [Saunders et al. 2000] provide two masks to account for the areas not completely observed, the smaller one leaving 84% of the sky, and the conservative one 72%.

1.4 Goal

A very common way to reconstruct or express a field is to expand it in a set of basis functions. If these basis functions are orthonormal it will be in principle straightforward to compute the expansion coefficients, and in addition they will be statistically independent. The presence of the mask and the selection function destroys the orthonormality of standard sets of basis functions like Fourier Modes or Spherical Harmonics and Spherical Bessel Functions, it is difficult or impossible to recover the single expansion coefficients, they get “mixed”.

The goal of this thesis is to construct a set of basis functions that are orthonormal in the presence of the mask and the selection function, so that their coefficients are straightforward to compute and statistically independent. As a first application we will reconstruct the overdensity field of our cosmological “neighbourhood” from the PSCz catalogue in redshift space.

In chapter 2 we will introduce the method we want to use. In chapter 3 we will describe tests of the method and explain some details in the application to the data. In chapter 4 we will present and discuss the results of our work, and chapter 5 we will give a general summary and outline of how this work could be extended.

Chapter 2

The Method

In order to reconstruct the continuous density field from the coordinates and apparent magnitudes of a finite number of galaxies one needs to consider several aspects.

Since the PSCz catalogue is flux (or apparent magnitude) limited it will not contain faint distant galaxies, as they will not be bright enough to be detected. Furthermore the apparent magnitude of a given galaxy is a decreasing function of distance, which means that a galaxy with a certain absolute magnitude can be detected if it is within some distance r , but will not be detected if it is situated in a larger distance. This feature is described by the selection function $\phi(r)$ which is defined as the fraction of the number of galaxies which meet the selection criteria of the catalogue at the distance r . It is essential to find the selection function for further analysis.

We account for the shot noise because a galaxy catalogue contains only a finite number of sampling points of the continuous underlying density field, and any process going from this finite set to the continuous field will introduce shot noise.

Another important point to consider is the mask, because in many cases a true full sky survey would be much easier to handle. To ignore the mask would introduce systematic errors.

In section 2.1 of this chapter we will introduce some methods that have been used so far to deal with these problems, and in sections 2.2 to 2.5 we will explain in detail the method we have explored here. Section 2.6 will summarise the most important points of this method.

2.1 Some Background Details

2.1.1 Selection Function and Luminosity Function

The selection function is strongly related to the luminosity function (see section 2.2). The luminosity function (LF) $f(M)$ describes the population of galaxies, so $f(M)dM$ is the fraction of the number of galaxies with apparent magnitudes between M and $M + dM$. In some cases it becomes more useful to work with the cumulative luminosity function (CLF) $F(M)$ instead of the LF itself. This function is called “luminosity function” because it also expresses the distribution in luminosity L ; the absolute magnitude M is just the logarithm of L : $M = -2.5 \cdot \log_{10} L - \text{const.}$ There are a variety of methods to estimate the LF or the CLF. Early methods (e.g. the $1/V_{max}$ method by [Schmidt 1968]) assumed a homogeneous galaxy distribution for the estimation. As we know of strong clustering properties it is better to use estimators that are not sensitive to inhomogeneities. There are several parametric forms for the LF, CLF and the selection function, e.g. by [Schechter 1976], [Yahil et al. 1991], and [Saunders et al. 2000].

The advantage of non-parametric estimation is that the functional form is completely free from assumptions. A well-known method is the C^- -method by [Lynden-Bell 1971]. It does not assume a homogeneous density, only that the LF is universal.

Several others have investigated the universality of the LF. [Springel and White 1998] report evolution in the LF, but [Teodoro 1999] shows that these effects become important only for distances of more than 200Mpc.

2.1.2 Smoothing Procedure

To convert the point distribution of the galaxies into a continuous density field a smoothing procedure could be applied, e.g.

$$\delta(\vec{r}) = \frac{1}{N_{gal}} \sum_{galaxies} \frac{W(|\vec{r} - \vec{r}_{galaxy}|/r_{smooth})}{\phi(r_{galaxy})} - 1, \quad (2.1)$$

where r_{smooth} is the smoothing length, and W is the normalised window function

$$\int W(r/r_{smooth})d^3r = 1. \quad (2.2)$$

Common window functions are the tophat, parabolic and Gaussian window functions. Because the data will be more sparse at larger distances one can increase the smoothing length with distance. Another option is to use an adaptive smoothing length that is proportional to the local interparticle separation (e.g. in [Fisher et al. 1995]). The described smoothing

procedure means that effectively one puts $1/\phi(r)$ galaxies at the position \vec{r} of a galaxy. For large r the selection function $\phi(r)$ can be very small and $1/\phi(r)$ large, so this is quite a simple approximation.

2.1.3 Expansion in Orthonormal Functions

Another standard approach is to expand the density field in a set of orthogonal functions, e.g. a Fourier Series or Spherical Harmonics and Spherical Bessel Functions, and find the coefficients for the expansion from the galaxy distribution.

A function $A(\vec{r})$ can be expanded in any complete set of linearly independent functions (basis functions) $\{f_i(\vec{r})\}$:

$$A(\vec{r}) = \sum_i A_i f_i(\vec{r}) \quad (2.3)$$

If the functions are orthonormal, that means if they satisfy the relation

$$\langle f_i, f_j \rangle = \delta_{ij}^K \quad (2.4)$$

(the δ^K denotes the Kronecker-delta; \langle, \rangle denotes a scalar product, $\langle f, g \rangle = \int f g d^3r$), it is straightforward to find the expansion coefficient A_j for the function $A(\vec{r})$. It is simply the scalar product of the function and the j th basis function:

$$\langle A, f_j \rangle = \langle \sum_i A_i f_i, f_j \rangle = \sum_i A_i \langle f_i, f_j \rangle = \sum_i A_i \delta_{ij}^K = A_j \quad (2.5)$$

If the data allows us to compute or to approximate these scalar products, the original function $A(\vec{r})$ can be reconstructed from the coefficients and the orthonormal basis functions.

The geometry of the task one wants to solve can give a hint which set of basis functions would be a good choice. E.g. in the case of a volume limited sample a Fourier series can simplify calculations, or in the case of a spherical symmetry the Spherical Harmonics and Spherical Bessel Functions can be useful.

2.1.4 The Mask

Of course a true full-sky survey would be the ideal data set, but the parts of the sky that are obscured by the Milky Way are very difficult to observe.

The incomplete sky coverage makes many calculations very cumbersome. Since in the PSCz survey only 28% of the sky (or if the smaller mask is used only 16%) is unobserved, it is possible to fill the masked regions artificially, using information from the observed region. An elementary way would be to fill the masked parts just with the mean galaxy number

density. One could also clone from adjacent observed regions as [Lynden-Bell et al. 1989] have suggested. An even more sophisticated way is to interpolate over the unsurveyed zone. Such a procedure is described in [Yahil et al. 1991] and was also applied by [Fisher et al. 1995] and [Teodoro 1999].

However, one introduces some artificial information into the analysis, and then has to quantify how far this influences the results.

2.1.5 Shot Noise

As already mentioned we will have to deal with shot noise because we convert a finite number of data points into a continuous field. The recovery of the coefficients is an inverse problem, and the existence of the noise makes a “direct” inversion unreliable, because during the “forward” process from the underlying field to the measurement some information has become blurred or was lost. There are several different ways to find a good estimate for the underlying field, and many of them make use of some a priori information. We will use the techniques of Singular Value Decomposition and Linear Regularisation, which will be described later. As an example of another method we give a short summary of Wiener Filtering.

Example: Wiener Filtering

A very simple example illustrating the principle of the Wiener Filter (for a more detailed review see e.g. [Press et al. 1992]) is the following one: Let s be a true underlying signal, and d some measurement of this signal. The measurement is corrupted by some noise σ in the sense that $d = s + \sigma$. The signal and the noise are uncorrelated, so that $\langle s\sigma \rangle = 0$. One can then try to find an estimate of the true signal \hat{s} by filtering the data: $\hat{s} = Fd$. The linear filter F can be optimised in different ways. One can assume that both s and σ are Gaussian distributed and ask the filter to maximise the conditional probability of \hat{s} given the measurement d , that is to yield the most likely estimate for \hat{s} given d ; one might also want to find the filter that minimises the variance between the true signal and the estimated one $\langle (s - Fd)^2 \rangle = \text{minimum}$. In both cases the filter will be the same, but in the latter case no assumption about the form of the probability distribution is made:

$$F = \frac{\langle s^2 \rangle}{\langle s^2 \rangle + \langle \sigma^2 \rangle} \quad (2.6)$$

This filter is often referred to as “signal/(signal +noise)”; and it requires an a priori knowledge of the variances of the signal and the noise.

[Lahav et al. 1994] and [Zaroubi et al. 1995] extend the application of the Wiener filter to the more complex case of the reconstruction of the density field. The principle however remains the same.

Let \vec{s} be a set of figures representing the signal we want to recover (e.g. the set of coefficients), and \vec{d} the set of data points one finds by measurement, which are linked by the following relation:

$$\vec{d} = R\vec{s} + \vec{\epsilon} \quad (2.7)$$

The matrix R represents a known “response function”. The statistical errors ϵ_j are uncorrelated with the underlying signal. In certain circumstances it becomes more useful if the noise is written as $\vec{\epsilon} = R\vec{\sigma}$. If the mean value and the covariance matrix $S = \langle \vec{s}\vec{s}^+ \rangle$ of the signal and the covariance matrix $N_\sigma = \langle \vec{\sigma}\vec{\sigma}^+ \rangle$ or $N_\epsilon = \langle \vec{\epsilon}\vec{\epsilon}^+ \rangle = RN_\sigma R^+$ of the noise can be found, it is possible to construct a filter matrix F that is applied to the data to obtain an estimate of the underlying signal:

$$\hat{\vec{s}} = F\vec{d} \quad (2.8)$$

[Zaroubi et al. 1995] show that in order to minimise the residual $\langle \vec{r}\vec{r}^+ \rangle = \langle (\vec{s} - \hat{\vec{s}})(\vec{s}^+ - \hat{\vec{s}}^+) \rangle$ the filter F is

$$F = SR^+(RSR^+ + N_\epsilon)^{-1} = S(S + N_\sigma)^{-1}R^{-1}. \quad (2.9)$$

The second version shows clearly the two operations the filter performs: the matrix R is inverted and the noise is suppressed (again we have the form “signal/(signal + noise)”). Calculations can be simplified if the noise and signal matrices N and S are diagonal. This is the case e.g. if the signal \vec{s} is the coefficients of a set of orthonormal functions. Then the diagonal elements of the signal matrix $S_{ii} = \langle s_i^2 \rangle$ are related to the power spectrum of the density fluctuations (clearly, in the case of a non-diagonal signal matrix all its elements are related to the power spectrum). So in order to apply a Wiener Filter one needs to assume a power spectrum a priori.

[Zaroubi et al. 1995] show that in the case of Gaussian random fields the Wiener Filter also yields the conditional mean field and in this case also the Bayesian estimator corresponds to the minimum variance estimator.

2.1.6 A Short Outline of our Method

For the estimation of the selection function we use a statistical description of the data. We derive an equation that allows us to estimate the cumulative luminosity function, which can

be used to find the selection function. The method is non-parametric and assumes a universal luminosity function.

The approach we then adopt is to reconstruct the density field by expanding it in Spherical Harmonics and Spherical Bessel Functions (SH&SB). As already mentioned, these functions are orthonormal on the full space, which is the property that makes it straightforward in principle to find the expansion coefficients. Unfortunately they are not orthogonal in the presence of the angular mask and the selection function, so the simple equation for computing the coefficients is no longer valid. We treat the selection function as a “radial mask”, and construct a set of functions that are orthonormal on the “radial and angular masked” space (short: masked space, MS). These functions are a linear combination of the SH&SB, and as a result of the orthonormality it is straightforward to compute their coefficients. This procedure avoids filling the mask with artificial information and it incorporates the selection function information in a more sophisticated way. The coefficients of the orthonormal basis can be transformed back to the ones of the SH&SB.

We handle the shot noise by inverting the transformation matrix via Singular Value Decomposition and we apply a linear regularisation technique.

In section 2.2 we will explain the method we use to find the selection function, in section 2.3 we will briefly introduce SH and SB and describe the construction of the orthonormal functions on the masked space. In section 2.4 we give a brief summary of Singular Value Decomposition, and in section 2.5 we will explain the concept of Linear Regularisation.

2.2 Reconstructing the Selection Function

Assuming that the angular and radial selection criteria of the PSCz catalogue can be separated, the selection function $\phi(r)$ is defined as the fraction of the number of galaxies that meet the selection criteria of the catalogue at distance r .

If the only radial selection criterion is the limit in apparent magnitude, $\phi(r)$ can be computed using the CLF $F(M)$. The CLF is defined as

$$F(M) = \int_{-\infty}^M f(M') dM'. \quad (2.10)$$

The function $f(M)$ is the LF, and $f(M)dM$ is the fraction of galaxies with absolute magnitude between M and $M+dM$ in an arbitrary volume. That means $F(\tilde{M})$ is the fraction of galaxies with $M \leq \tilde{M}$, the fraction of galaxies brighter than \tilde{M} .

Due to the limited sensitivity of the measurements the catalogue contains only galaxies

with apparent magnitude brighter than m_{lim} , which means that at a given distance r only galaxies with $M \leq M_{lim}(r)$ (see section 2.2.2) are included. Thus we can compute $\phi(r)$ according to this selection criterion:

$$\phi(r) = F(M_{lim}(r)). \quad (2.11)$$

2.2.1 K-Correction

For analysing the IRAS PSCz catalogue we first need to know the “true apparent” or bolometric magnitude m_{bol} of the galaxies. As defined in [Humason et al. 1956, appendix B] this is the total energy, expressed as a magnitude, received from all wavelengths on a unit area outside the earth’s atmosphere.

The measured apparent magnitude m_m differs from m_{bol} for two reasons. One is the wavelength dependent sensitivity of the instrument (and in case of measurements from the earth’s surface the transmission of our atmosphere). The second arises because due to the redshift all emitted wavelengths are shifted to $\lambda_{observed} = \lambda_{emitted}(1 + z)$, but the measurement uses a filter of fixed bandwidth.

The correction which takes account of these two effects is called K-correction. Let us define the correction in the following way:

$$m_{bol}(z) = m_m - \Delta(z), \quad (2.12)$$

where $\Delta(z)$ is the redshift dependent correction term and m_m the measured apparent magnitude of a galaxy at redshift z , defined by

$$m_m = -2.5 \log_{10} \left[A \int_0^{+\infty} S(\lambda) f_z(\lambda) d\lambda \right]. \quad (2.13)$$

A is a normalization constant depending on the zero point of the magnitude scale. The function $S(\lambda)$ describes the sensitivity of the instrument (and transmission of the atmosphere, if measurements are ground based). The function $f_z(\lambda)$ is the spectral energy distribution (SED) of the galaxy at redshift z as it would be measured outside our atmosphere. So $f_0(\lambda)$ could be called the “true” SED.

The term $\Delta(z)$ is hard to compute, but we can reduce it to terms which can be computed by “adding a zero”:

$$m_{bol}(z) = m_m - \Delta(0) - K \quad (2.14)$$

$$\text{with } K \equiv \Delta(z) - \Delta(0) \quad (2.15)$$

Using intensities instead of magnitudes in eqn. 2.12 and recalling the definition of K yields

$$I_{bol}(z) = I_m(z)10^{0.4\Delta(z)} \quad \text{and} \quad (2.16)$$

$$\frac{I_{bol}(z)}{I_{bol}(0)} = \frac{I_m(z)}{I_m(0)}10^{0.4K} \quad (2.17)$$

This means

$$K = 2.5 \log_{10} \frac{I_{bol}(z)}{I_{bol}(0)} + 2.5 \log_{10} \frac{I_m(0)}{I_m(z)}. \quad (2.18)$$

The two expressions on the rhs can be computed as follows. By definition

$$\frac{I_{bol}(z)}{I_{bol}(0)} = \frac{\int_0^{+\infty} f_z(\lambda) d\lambda}{\int_0^{+\infty} f_0(\lambda) d\lambda}. \quad (2.19)$$

Of course the SED $f(\lambda)$ has to be a “well-behaved” function in the sense that the integrals do not diverge. If one knows the “true” SED $f_0(\lambda)$, one can determine $f_z(\lambda)$ by plotting the value of $f_0(\lambda')$ at $\lambda_{new} = (1+z)\lambda'$. This means the area under the curve $f_z(\lambda)$ increases by a factor of $(1+z)$, so the first expression in eqn. 2.18 is $2.5 \log_{10}(1+z)$.

If you assume a power law for the “true” SED $f_0(\nu) \propto \nu^{-\beta} \propto \lambda^{\beta-2}$ (in a certain spectral range and $f(\lambda) = 0$ elsewhere; otherwise the integral over $f(\lambda)$ would diverge), it is straightforward to compute the second expression of eqn. 2.18:

$$\frac{I_m(0)}{I_m(z)} = \frac{\int_0^{+\infty} S(\lambda) f_0(\lambda) d\lambda}{\int_0^{+\infty} S(\lambda) f_z(\lambda) d\lambda} = \frac{\int_0^{+\infty} S(\lambda) \lambda^{\beta-2} d\lambda}{\int_0^{+\infty} S(\lambda) \lambda^{\beta-2} (1+z)^{-(\beta-2)} d\lambda} = (1+z)^{(\beta-2)} \quad (2.20)$$

In this case we get

$$K = 2.5(\beta - 1) \log_{10}(1+z) \quad (2.21)$$

and assuming that $\Delta(0)$ is zero for the PSCz galaxies (which just means that a correction is not necessary for galaxies with $z = 0$)

$$m_{bol}(z) = m_m(z) - \Delta(z) \quad \text{with} \quad \Delta(z) = 2.5(\beta - 1) \log_{10}(1+z) \quad (2.22)$$

So the corrected version of the equation relating the absolute magnitude, the apparent magnitude and the distance modulus μ is

$$\mu = m_m - M - \Delta(z) \quad (2.23)$$

For the K -correction the redshift in the heliocentric rest frame z_H should be used.

2.2.2 Luminosity Function

For reconstructing the CLF $F(M)$ of the galaxies we use a method related to the C^- -Method of [Lynden-Bell 1971]. The statistical treatment which is used was introduced in [Rauzy and Hendry 2000]. For the explanation first we neglect the K -correction.

We assume that the luminosity function $f(M)$ is independent of the spatial position $\vec{r} = (r, l, b)$, i.e., that it is universal. In this case the PSCz sample can be described by the probability density dP

$$dP_{r,b,l,M} \propto \rho(r, l, b) M(l, b) r^2 \cos b \, dl db dr f(M) dM \Theta(m_{lim} - m), \quad (2.24)$$

where ρ is the spatial distribution function of the galaxies. $\Theta(x)$ is the Heaviside step function, it expresses the fact that the catalogue does not include galaxies with apparent magnitude fainter than m_{lim} . $M(l, b)$ is the angular mask.

Changing coordinates from r to the distance modulus $\mu = m - M = 5 \log_{10} r + 25$

$$dP_{\mu,b,l,M} \propto h(\mu, l, b) M(l, b) \cos b \, dl db d\mu f(M) dM \Theta(m_{lim} - m). \quad (2.25)$$

and integrating over l and b leads to

$$dP_{\mu,M} = \frac{1}{A} h(\mu) d\mu f(M) dM \Theta(m_{lim} - m). \quad (2.26)$$

A is the normalisation constant, and $h(\mu, l, b) d\mu = \rho(r(\mu), l, b) r^2 dr$.

Let us define $\mu_{lim} \equiv \mu_{lim}(M) = m_{lim} - M$ and $H(\mu) \equiv \int_{-\infty}^{\mu} h(\mu') d\mu'$ and the new random variable

$$\zeta_{\mu} \equiv \frac{H(\mu)}{H(\mu_{lim}(M))}. \quad (2.27)$$

Changing coordinates again from μ to ζ_{μ} we have to rewrite the volume element according to

$$d\zeta_{\mu} dM = \frac{h(\mu)}{H(\mu_{lim}(M))} d\mu dM, \quad (2.28)$$

the probability distribution may be written

$$dP_{\mu,M} = \frac{1}{A} \frac{h(\mu)}{H(\mu_{lim}(M))} d\mu f(M) H(\mu_{lim}(M)) dM \Theta(\mu_{lim} - \mu) \quad (2.29)$$

$$= \Theta(1 - \zeta_{\mu}) \Theta(\zeta_{\mu}) d\zeta_{\mu} \frac{1}{A} f(M) H(\mu_{lim}(M)) dM \quad (2.30)$$

Due to its definition ζ_{μ} is uniformly distributed between 0 and 1, which is expressed by the two Heaviside functions in the last eqn. So integrating over ζ_{μ} just yields

$$dP_M = \frac{1}{A} f(M) H(\mu_{lim}(M)) dM. \quad (2.31)$$

Now we define N_M , the number of galaxies with $M \leq M_i$ and $\mu \leq \mu_{lim,i}$ (see also figure 2.1). The ratio of N_M and the total number of galaxies in the sample N_{tot} can be expressed by integrating over $dP_{\mu',M'}$

$$\frac{N_M}{N_{tot}} = \int_{-\infty}^{\mu_{lim}} \int_{-\infty}^M dP_{\mu',M'} = \frac{1}{A} H(\mu_{lim}(M)) F(M). \quad (2.32)$$

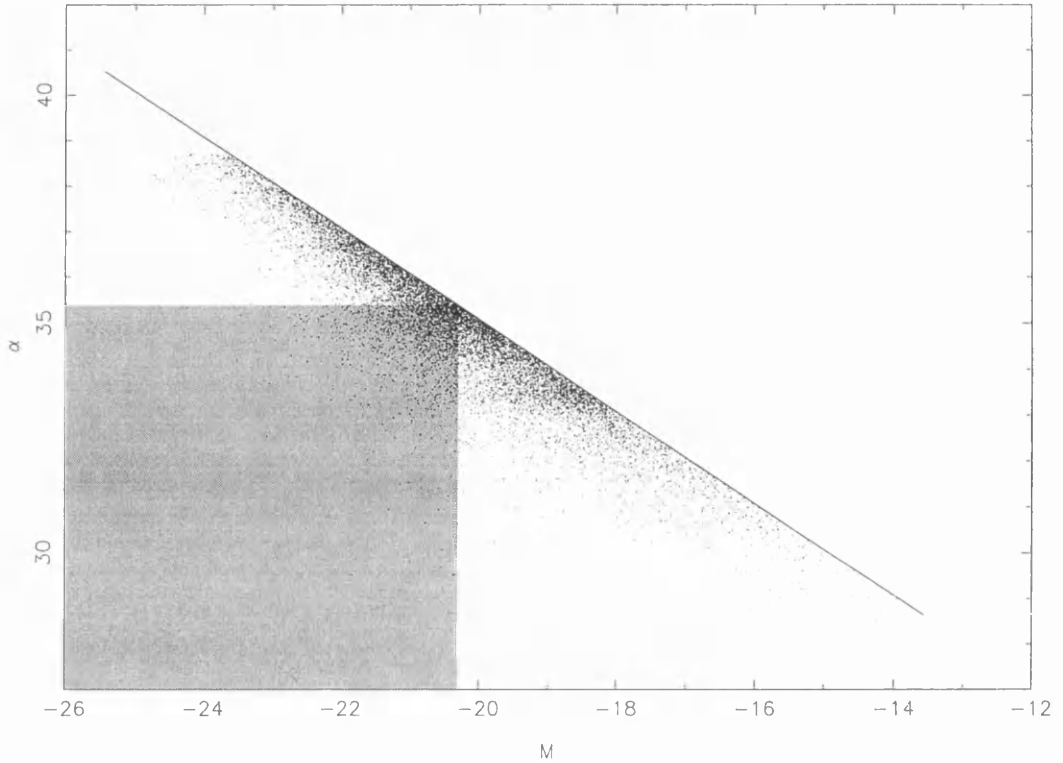
PSCz-galaxies in M- α -Plot

Figure 2.1: Absolute magnitude M versus α plot for the PSCz-galaxies. α is the uncorrected distance modulus. The method is illustrated, for example $N_{M=-20.5}$ is the number of galaxies in the shaded area.

From this eqn. and eqn. 2.31 we get

$$dP_M = \frac{N_M}{N_{TOT}} d(\ln F(M)) \quad (2.33)$$

The numbers N_M can be counted from an M - μ -plot of the sample. Using the weighting function $w(M) = \frac{N_{tot}}{N_M}$, the integral $\int_{M_0}^M w(M') dP_{M'}$ can be evaluated on the one hand but can be approximated on the other hand by

$$\frac{1}{N_{tot}} \sum_{M_i \leq M} w(M_i) \approx \int_{M_0}^M w(M') dP_{M'} = \int_{M_0}^M d(\ln F(M')) = \ln F(M) - const. \quad (2.34)$$

So this relationship makes it possible to estimate $\ln F(M)$:

$$\ln F(M) = \sum_{M_i \leq M} \frac{1}{N_{M_i}} + const. \quad (2.35)$$

When we compute the N_{M_i} for the galaxy i we can choose to include galaxy i or to exclude it, because this theory also works for counting the galaxies with $M < M_i$ and $\mu < \mu_{lim,i}$.

This would lead to

$$\ln F(M) = \sum_{M_i \leq M} \frac{1}{(N_{M_i} - 1)} + \text{const.} \quad (2.36)$$

To account for this we use in our analysis

$$\ln F(M) = \sum_{M_i \leq M} \frac{1}{N_{M_i} - 0.5} + \text{const.} \quad (2.37)$$

Now we have to consider the K-correction. If we do this, we cannot define a unique $\mu_{lim}(M)$, because μ_i have to be computed according to eqn. 2.23 for each galaxy, and two galaxies with the same M could have two different μ_{lim} . We can avoid that problem if we take an M - α -plot of the sample instead of an M - μ -plot, where $\alpha = m_m - M = \mu + \Delta(z)$ is the uncorrected distance modulus. There is a unique $\alpha_{lim} = m_{lim} - M$ for each M . So the method stays the same but N_M is the number of galaxies in the analogous area in the M - α -plot of the sample (see also figure 2.1).

When computing the selection function from the CLF we follow equation 2.11 with $M_{lim} = m_{lim} - \mu(r(z)) - \Delta(z)$ (taking into account the K-correction).

2.3 Expanding the Density Field

2.3.1 Spherical Harmonics and Spherical Bessel Functions

We use spherical coordinates (r, θ, φ) or galactic coordinates (r, l, b) to express the position of a galaxy in space. The PSCz catalogue has spherical symmetry, so it is a natural choice to decompose the density field in SH&SB. In this context another advantage of the SH&SB is that radial and angular effects (e.g. the angular mask and the selection function and the radial distortion due to peculiar motions) can be separated.

A field $A(\vec{r})$ can be expanded in SH $Y_{lm}(\theta, \phi)$ and SB $j_l(k_{ln}r)$ in the following way:

$$A(\vec{r}) = \sum_{n=1}^{\infty} \sum_{l=0}^{\infty} \sum_{m=-l}^l A_{nlm} \cdot c_{ln} j_l(k_{ln}r) Y_{lm}(\theta, \varphi) \quad \text{with} \quad (2.38)$$

$$A_{nlm} = \int_{\text{observed volume}} A(\vec{r}) \cdot c_{ln} j_l(k_{ln}r) Y_{lm}(\theta, \varphi) d^3r \quad (2.39)$$

The observed volume is a sphere with radius R_{max} . The factor c_{ln} is a normalisation constant which appears in both the expansion and the coefficients as in [Heavens and Taylor 1995]. The function $j_l(x)$ is the SB of order l ; it is related to the Ordinary Bessel function $J_\nu(x)$ by $j_l(x) = \sqrt{\pi/(2x)} J_{l+1/2}(x)$. Often SH contain imaginary parts as defined as in [Binney and Tremaine 1987]. Because we want to work later with the method of [Gorski 1994],

we will adopt his definition, which is a “reorganisation” so that the SH are real:

$$Y_{lm} = \sqrt{\frac{2l+1}{4\pi} \frac{(l-|m|)!}{(l+|m|)!}} P_l^{|m|}(\cos\theta) \cdot f(\varphi)$$

$$\text{with } f(\varphi) = \begin{cases} 1 & m = 0 \\ \sqrt{2} \cos(m\varphi) & \text{for } m > 0 \\ \sqrt{2} \sin(|m|\varphi) & m < 0 \end{cases} \quad (2.40)$$

The functions $P_l^m(x)$ are the Associated Legendre Polynomials.

The radial wavenumbers k_{ln} can be found from a boundary condition. The normalisation constants c_{ln} can be calculated using the orthogonality relations for the Spherical Harmonics and Bessel Functions. Our choice of the boundary condition will be explained in section 3.2.

For a shorter notation we define

$$\Upsilon_{nlm}(r, \theta, \varphi) \equiv c_{ln} j_l(k_{ln} r) Y_{lm}(\theta, \varphi). \quad (2.41)$$

As already mentioned, the functions Υ_{nlm} are orthonormal on a spherical volume with radius R_{max} with respect to the scalar product $\langle f, g \rangle \equiv \int f g d^3r$, which reads in the new notation

$$\langle \Upsilon_{n'l'm'}, \Upsilon_{nlm} \rangle \equiv \int_{obs. v.} \Upsilon_{n'l'm'}(r, \theta, \varphi) \cdot \Upsilon_{nlm}(r, \theta, \varphi) d^3r = \delta_{nn'}^K \delta_{ll'}^K \delta_{mm'}^K. \quad (2.42)$$

Usually the scalar product is defined as $\langle f, g^* \rangle$, and the Spherical Harmonics used by e.g. [Heavens and Taylor 1995] and [Binney and Tremaine 1987] are only orthonormal in this scalar product, because they contain imaginary parts. The functions we use are real, so the scalar product reduces to $\langle f, g^* \rangle = \langle f, g \rangle$.

The orthonormality makes it easy to find the coefficients according to eqn. 2.39, which can be written in the new notation as

$$A_{nlm} = \langle A(\vec{r}), \Upsilon_{nlm} \rangle = \int_{obs. v.} A(r, \theta, \varphi) \Upsilon_{nlm}(r, \theta, \varphi) r^2 \sin\theta dr d\theta d\varphi. \quad (2.43)$$

2.3.2 Problems due to the Mask and the Selection Function

We cannot observe the complete sphere to a limiting radius. The PSCz-catalogue has an angular mask which covers unobserved regions. In addition to this angular mask there is the selection function which could be called a “radial mask” for the PSCz catalogue. These two masks together mean that we can only work in a “masked space” (MS), this expression will be used for the angular and radial mask together.

In the case where $A(\vec{r})$ is the galaxy number density field $\rho(\vec{r})$ one would like to approximate the integral in eqn. 2.43, which is the scalar product on the unmasked or full space, by

a sum over $\Upsilon_{nlm}(r, \theta, \varphi)$ over all galaxies, but due to the selection function and the angular mask this sum actually approximates a different integral:

$$\frac{1}{N_{gal}} \sum_{galaxies} \Upsilon_{nlm}(\vec{r}_{galaxy}) \approx \int \Upsilon_{nlm}(\vec{r}) dP \quad (2.44)$$

$$\text{with } dP = \frac{1}{K} \rho(\vec{r}) \cdot M(\theta, \varphi) \cdot \phi(r) d^3r, \quad (2.45)$$

where K is a normalisation constant. The function $M(\theta, \varphi)$ codes the angular mask ($M = 1$ if the direction is outside the angular mask, $M = 0$ if the direction is covered by the angular mask), $\phi(r)$ is the selection function, so dP is the probability that we observe a galaxy in the volume d^3r at the position \vec{r} . As ρ is the galaxy number density, the constant K will be the number of observable galaxies in the observed volume given the mask and the selection function, or $K = N_{gal}$. We can define a new scalar product for real functions

$$\langle f, g \rangle_{[MS]} \equiv \int_{\text{obs. v.}} f(\vec{r}) g(\vec{r}) M(\theta, \varphi) \phi(r) d^3r, \quad (2.46)$$

and the sum in eqn. 2.44 does approximate this scalar product:

$$\sum_{galaxies} \Upsilon_{nlm}(\vec{r}_{galaxy}) \approx \langle \rho(\vec{r}), \Upsilon_{nlm} \rangle_{[MS]} \quad (2.47)$$

Unfortunately the functions Υ_{nlm} are not orthogonal with this scalar product (“on the masked space”), so it is not possible to find the coefficients ρ_{nlm} according to the last eqn.

2.3.3 Dealing with the Mask and the Selection Function

[Gorski 1994] demonstrated a method to deal with such a problem. He showed how a set of functions which are orthonormal on the masked space can be constructed and how these can be used to derive the desired coefficients. He applied the method to the two-dimensional problem of analysing the COBE CMB data, but it is straightforward to extend to three dimensions.

In practice one cannot expand the series up to an infinite number of coefficients, so we need to find an l_{max} and an n_{max} . Criteria for choosing them are explained in section 3.2. First the functions Υ_{nlm} are sorted in a vector $\vec{\Upsilon}$ so that we can label them by a single index i . We adopt the following ordering, but there are other possibilities:

$$\begin{aligned} \vec{\Upsilon} = & (\Upsilon_{1,0,0}, \Upsilon_{1,1,-1}, \Upsilon_{1,1,0}, \Upsilon_{1,1,1}, \Upsilon_{1,2,-2}, \Upsilon_{1,2,-1}, \dots, \Upsilon_{1,l_{max},l_{max}}, \\ & \Upsilon_{2,0,0}, \Upsilon_{2,1,-1}, \Upsilon_{2,1,0}, \dots, \Upsilon_{n_{max},l_{max},l_{max}}) \end{aligned}$$

Thus, from the position in this vector, which is the single index i , the three indices n, l, m of the function Υ_i can be found by:

$$n = (\text{integer}) \frac{i-1}{(l_{max}+1)^2} + 1 \quad (2.48)$$

$$l = (\text{integer}) \sqrt{i - (n-1)(l_{max}+1)^2 - 1} \quad (2.49)$$

$$m = i - (n-1)(l_{max}+1)^2 - l^2 - l - 1 \quad (2.50)$$

where the operator (integer) denotes to take the integer part. Now we define the matrix \tilde{W} with the elements $\tilde{W}_{ij} = \langle \Upsilon_i, \Upsilon_j \rangle_{[\text{unmasked space}]}$. Remembering that the functions Υ_i are orthonormal it is obvious that the matrix \tilde{W} must be the identity matrix I .

The coupling matrix W with elements

$$W_{ij} = \langle \Upsilon_i, \Upsilon_j \rangle_{[MS]} \quad (2.51)$$

is not the identity matrix because the Υ_i are not orthogonal on the masked space. The matrix W will not be diagonal, but symmetric, positive definite and nonsingular. The check for positive definiteness is straightforward, it makes use of the fact that the matrix elements are scalar products themselves and that the “weight” that distinguishes the scalar products on the full space and on the masked space (i.e. $M(\theta, \varphi)\phi(r)$) is non-negative, and therefore the squareroot of it can be taken:

$$\begin{aligned} \vec{v}^T W \vec{v} &= \sum_{ij} v_i W_{ij} v_j = \langle \sum_i v_i \Upsilon_i, \sum_j v_j \Upsilon_j \rangle_{[MS]} \\ &= \langle f, f \rangle_{[MS]} \quad \text{with } f = \sum_i v_i \Upsilon_i \\ &= \langle \sqrt{M\phi} f, \sqrt{M\phi} f \rangle_{[\text{unmasked space}]} > 0 \end{aligned} \quad (2.52)$$

The scalar product in the last line could only be zero if and only if the function $f \neq 0$ only where $M\phi = 0$. Because f is a finite linear combination of the analytic SH&SB, this case is excluded by construction and the matrix W is positive definite. Therefore it is also nonsingular.

Due to these properties the matrix W can be Choleski-decomposed into a lower triangular matrix L and its transpose L^T

$$W = L \cdot L^T \quad (2.53)$$

Let Γ be the inverse matrix of L :

$$\Gamma = L^{-1}. \quad (2.54)$$

Γ is also a lower triangular matrix. With this matrix we can construct a new vector $\vec{\Psi}$ of functions Ψ_j by

$$\vec{\Psi} = \Gamma \cdot \vec{\Upsilon}. \quad (2.55)$$

We can compute the matrix Q with elements $Q_{ij} = \langle \Psi_i, \Psi_j \rangle_{[MS]}$. Eqns. 2.55 and 2.51 show that Q is the identity matrix:

$$\begin{aligned} Q_{ij} &\equiv \langle \Psi_i, \Psi_j \rangle_{[MS]} \\ &= \langle \sum_k \Gamma_{ik} \Upsilon_k, \sum_l \Gamma_{jl} \Upsilon_l \rangle_{[MS]} = \sum_{kl} \Gamma_{ik} \Gamma_{jl} \langle \Upsilon_k, \Upsilon_l \rangle_{[MS]} \\ &= \sum_{kl} \Gamma_{ik} \Gamma_{jl} W_{kl} = (\Gamma \cdot W \cdot \Gamma^T)_{ij} \end{aligned} \quad (2.56)$$

$$\text{which means that } Q = \Gamma \cdot W \cdot \Gamma^T = \Gamma \cdot L \cdot L^T \cdot \Gamma^T = I, \quad (2.57)$$

So the functions Ψ_j are orthonormal on the masked space. As the Ψ_j are a linear combination of the Υ_i , it is also possible to express the Υ_i as a linear combination of the Ψ_j . Due to the definitions of the matrices L and Γ the transformation is

$$\Upsilon_i = \sum_j L_{ij} \Psi_j. \quad (2.58)$$

Substituting this expression in eqn. 2.38 it is easy to see that the field $A(\vec{r})$ can also be expanded using the functions Ψ_j and the coefficients \tilde{A}_j :

$$A(\vec{r}) = \sum_j \tilde{A}_j \cdot \Psi_j \quad \text{with} \quad (2.59)$$

$$\tilde{A}_j = \sum_i L_{ji}^T A_i \quad (2.60)$$

The orthonormality of the functions Ψ_j on the masked space allows us to compute the coefficients \tilde{A}_j directly by

$$\tilde{A}_j = \langle A(\vec{r}), \Psi_j \rangle_{[MS]}. \quad (2.61)$$

Of course the coefficients \tilde{A}_j can be transformed back to the A_i by

$$A_i = \sum_j \Gamma_{ij}^T \tilde{A}_j, \quad (2.62)$$

and so the field can now be reconstructed with the coefficients A_i and the SH&SB or the \tilde{A}_j and the functions Ψ_j .

2.4 Singular Value Decomposition (SVD)

We need to invert a big matrix, and it often happens that due to roundoff errors, this matrix is very close to a singular matrix. This can lead to severe instability in the inversion. SVD

gives a powerful tool to stabilise the inversion. The SVD of a $M \times N$ matrix A (with $M \geq N$) finds three matrices U , W , and V with special properties. The matrix U is also an $M \times N$ matrix, W and V are $N \times N$ matrices. The matrices U and V are column orthogonal, W is diagonal, the elements w_i on this diagonal are positive or zero, they are the singular values of the matrix A . Furthermore, the matrix A is given by

$$A = U \cdot W \cdot V^T \quad (2.63)$$

If A is a square matrix, U , W , and V are also square matrices. Since U and V are orthogonal, their inverses equal their transposes; the inverse of the matrix W is a diagonal matrix with diagonal elements $1/w_i$. So the inverse of A is

$$A^{-1} = V \cdot [\text{diag}(1/w_i)] \cdot U^T \quad (2.64)$$

If the matrix A is singular or close to singular, one or more of the w_i will be zero or very small, so that the reciprocal $1/w_i$ is not defined or is very large. How severe the problem is can be seen from the condition number, which is the ratio of the largest to the smallest singular value. It turns out (see [Press et al. 1992] for details) that one can stabilise the inversion by replacing $1/w_i$ by zero if w_i is zero or smaller than $w_{i,max}/C$, where C is the “allowed maximum” for the condition number. One throws away some information.

Consider the mapping $A\vec{x} = \vec{b}$. If A is singular, its range is smaller than N . This means there is a subspace of vectors \vec{x} that are always mapped to zero by A : $A\vec{x} = 0$. Due to this fact there is also a subspace of vectors \vec{b} that can never be “reached” by the matrix A (there is no \vec{x} with $A\vec{x} = \vec{b}$ for these \vec{b}). For any \vec{b} , there are two possibilities: if \vec{b} is in the range of A , there is more than one solution for \vec{x} , and the truncated SVD inversion finds the solution with the smallest length $|\vec{x}|^2$. If \vec{b} is not in the range of A , formally there is no solution, but the truncated SVD inversion finds the vector \vec{x} which is the best solution in the sense that $|A\vec{x} - \vec{b}|$ is minimal. If the matrix A is nonsingular, but very close to singular, small changes in the vector \vec{b} will cause large changes in the solution \vec{x} , making the inversion unstable. The truncated SVD inversion throws away combinations of the data that are dominated by the roundoff errors or noise, and do not contain much useful information. Therefore the solution will be much more stable.

What condition number one allows has to be decided in each individual case. We explain the decision in our case in section 3.3.

2.5 Linear Regularisation

The technique of Linear Regularisation deals with recovering an underlying function from some measurements that can be described as a linear transform of the underlying function. Let u_μ be the set of underlying values one wants to recover, and c_i be the measurements one can take, each with a measurement error n_i , the measurements and underlying values are related by the response matrix $D_{i\mu}$:

$$c_i = \sum_{\mu} D_{i\mu} u_\mu + n_i \quad (2.65)$$

If the covariance matrix $S_{ij} = \text{Covar}[n_i, n_j]$ is known, one can try to find the set of estimators of the u_μ that minimize the χ^2 measure, which is a measure how well some model \hat{u}_μ agrees with the data:

$$\chi^2 = \sum_{ij} [c_i - \sum_{\mu} D_{i\mu} \hat{u}_\mu] S_{ij}^{-1} [c_j - \sum_{\mu} D_{j\mu} \hat{u}_\mu] \quad (2.66)$$

The matrix S_{ij}^{-1} is the inverse of the covariance matrix. When minimizing χ^2 one can find good agreement with the data, but the result can be unstable and can contain “statistical artefacts” and very large errors. Strong oscillations in the result are likely to be due to the noise rather than to the underlying physical process.

Therefore one can construct another positive functional Ξ that measures e.g. the “smoothness” of the reconstructed function. Then the idea of inverse theory (see [Press et al. 1992]) is to minimise not the measure for agreement (i.e. the χ^2), but

$$\text{minimise: } \chi^2 + \lambda \Xi \quad (2.67)$$

The functional Ξ includes some a priori information about the underlying field, such as its “smoothness”. The constant λ adjusts the “compromise” between good agreement with the data and the bias introduced by the a priori information.

How we will apply this technique to our specific problem will be described in section 3.4.

2.6 The Method summarised

In this section we list the principal steps which will be performed. More details will be given in chapter 3.

Selection Function

Compute for each galaxy i :

- K-correction: $\Delta_i(z) = 2.5(\beta - 1) \log_{10}(1 + z_i)$
- Absolute magnitude $M_i = m_i - \mu(r(z_i)) - \Delta(z_i)$
- quantity $\alpha_i = m_i - M_i = \mu_i + \Delta(z_i)$ and $\alpha_{lim,i} = m_{lim} - M_i$
- number N_{M_i} of galaxies with $M \leq M_i$ and $\alpha \leq \alpha_{lim,i}$

Then the CLF $F(M)$ can be computed for several M by

- $\ln F(M) = \sum_{M_i \leq M} \frac{1}{N_{M_i}^{-0.5}}$

And with $M_{lim}(r) = m_{lim} - \mu(r(z)) - \Delta(z)$ the selection function is

- $\phi(r) = F(M_{lim}(r))$

Gorski-Method

The goal is to expand the density field $\rho(\vec{r})$ in a set of basis functions Υ_i :

$$\rho(\vec{r}) = \sum_i \rho_i \Upsilon_i(\vec{r})$$

The basis functions $\Upsilon_i(\vec{r})$ are the SH&SB:

$$\Upsilon_i(r, \theta, \varphi) \equiv c_{ln} j_l(k_{ln} r) Y_{lm}(\theta, \varphi)$$

Therefore we need (details about constants and parameters will be given in chapter 3):

- The conversion between the single index i and the index triplet (n, l, m) :

$$n = (\text{integer}) \frac{i-1}{(l_{max}+1)^2} + 1$$

$$l = (\text{integer}) \sqrt{i - (n-1)(l_{max}+1)^2 - 1}$$

$$m = i - (n-1)(l_{max}+1)^2 - l^2 - l - 1$$

- The wavenumbers k_{ln} and the normalisation constants c_{ln}

- The matrix W with elements $W_{ij} = \langle \Upsilon_i, \Upsilon_j \rangle_{[MS]}$
- Perform Choleski decomposition to find the lower triangular matrix L so that $W = L \cdot L^T$
- Invert L via truncated Singular Value Decomposition, excluding small singular values
- Construct new set of functions $\Psi_j(\vec{r})$: $\Psi_j = \sum_i L_{ji}^{-1} \Upsilon_i$
- Compute coefficients R_j (the coefficients for the new set of basis functions) by $R_j = \langle \rho(\vec{r}), \Psi_j \rangle_{[MS]}$, with linear regularisation
- (Transform to the coefficients of the SH&SB: $\rho_i = \sum_j L_{ij}^{-1T} R_j$)
- Compute the density either with the SH&SB or with the new set of functions: $\rho(\vec{r}) = \sum_i \rho_i \Upsilon_i(\vec{r}) = \sum_j R_j \Psi_j(\vec{r})$

Chapter 3

Applying the Method to Data, Tests

Before we start to apply the method to the PSCz catalogue we need to translate the measured fluxes into apparent magnitudes. Therefore absolute luminosities are expressed in terms of the solar luminosity, leading to the transformation formula

$$m_m = -2.5 \log_{10} f_{60} + 30.0 - 2.5 \cdot \log_{10}(1.5608 \cdot 10^6) \quad (3.1)$$

The sensitivity limit of the flux measurements of $0.6 Jy$ ([Lawrence et al. 1999]) corresponds to a limit in apparent magnitude of $m_{lim} = 15.0731$.

The redshifts in the CMB frame were obtained by correcting the heliocentric redshifts for the motion of the sun with respect to the CMB ($v = 369.5 \text{ km s}^{-1}$, in the direction $l = 264.4^\circ$, $b = 48.4^\circ$, from [Yahil et al. 1977]; (l, b) are galactic coordinates).

To compute redshift distances r_s from redshifts z we assume a matter-dominated universe and convert all CMB-redshifts into luminosity distances $d_L(z_{CMB})$ following [Peacock 1999]

$$r_s = d_L = \frac{2c}{H_0 \Omega^2} [\Omega z_{CMB} + (\Omega - 2)(\sqrt{1 + \Omega z_{CMB}} - 1)]. \quad (3.2)$$

with $H_0 = 100h^{-1} \text{ km s}^{-1} \text{ Mpc}^{-1}$. These are redshift distances, they are not corrected for peculiar motions, because we work with redshift space coordinates \vec{r}_s and not real space coordinates \vec{r} .

In order to minimize small scale effects and non-linear effects we include in our analysis only galaxies with CMB-velocities of $500 \text{ km s}^{-1} \leq cz_{CMB} \leq V_{max} = 20,000 \text{ km s}^{-1}$. The choice of V_{max} depends on the fact that for large distances the catalogue contains only very few galaxies, so that it is not possible to extract much more reliable information from those. In

Mask and Galaxies of PSCz Catalogue

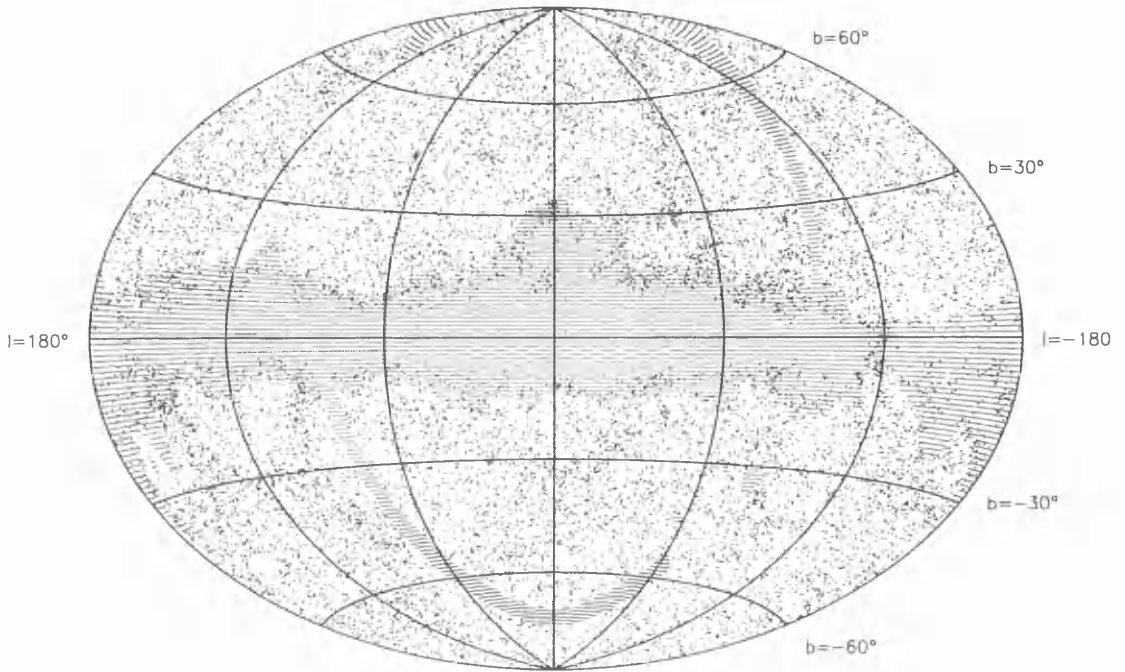


Figure 3.1: Used mask (grey shaded areas) and the PSCz galaxies.

addition, the range in which we found the selection function to be in good agreement with the data is also $V_{max} = 20,000 \text{ km s}^{-1}$ (see sections 3.1.1 and 4.1). Of course we need to exclude the galaxies behind the mask. This leaves 10654 galaxies from the original 14677.

We decided to use the larger mask of the PSCz catalogue to avoid errors that might arise from incomplete sampling and confusion with galactic sources near the galactic plane. Figure 3.1 shows the mask and all PSCz galaxies in an Aitoff projection using galactic coordinates, the galactic centre is at the centre of the plot. We exclude all galaxies that are in the grey shaded areas.

The radial distribution of the PSCz galaxies is shown in figure 3.2. The histogram in this plot shows the number of galaxies in each of 50 distance bins.

One important thing to mention is that the method which we used to determine the selection function only allows us to find its shape, not its normalisation. However, in the overdensity this unknown constant cancels, so we can ignore it there. Only when we compare the derived selection function to an assumed one or to one that was derived by different method, do we have to keep in mind that we still have the freedom to renormalise our selection function.

In section 3.1 we will describe testing and applying the reconstruction method for the selection function. In section 3.2 we will explain our choice of boundary condition and the

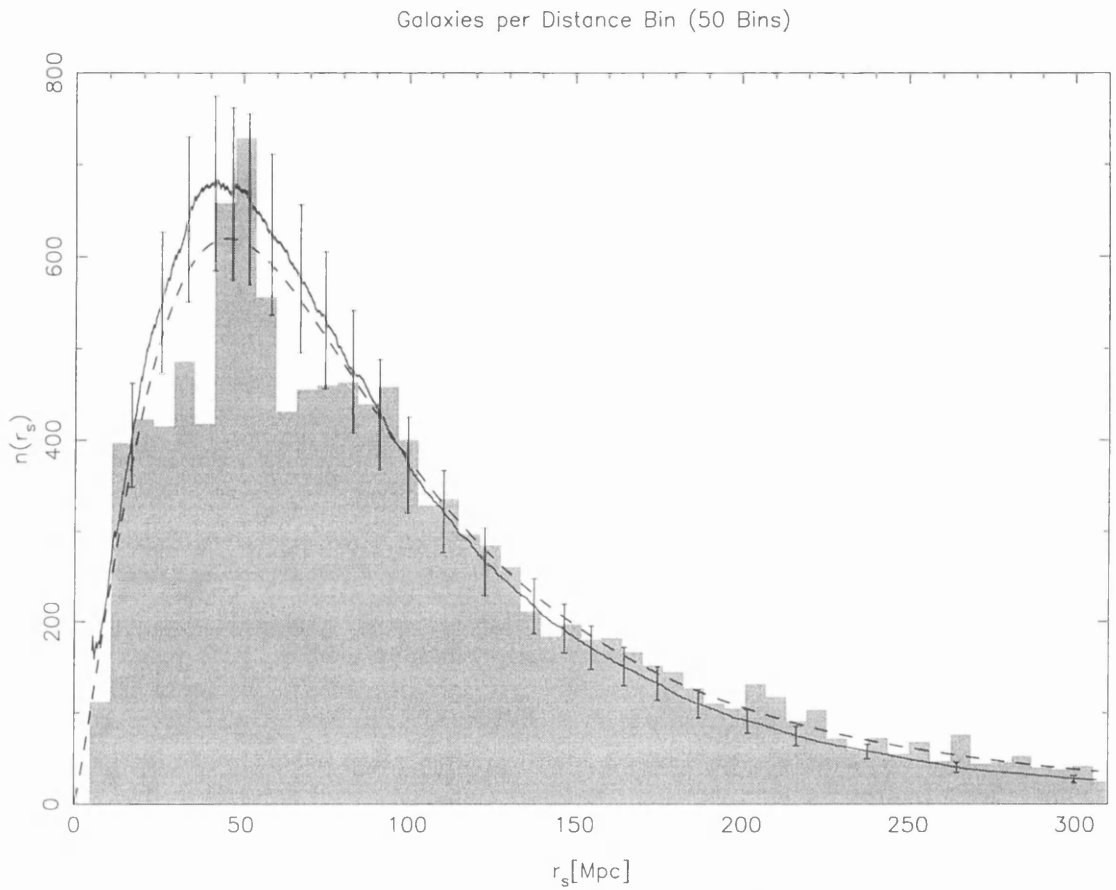


Figure 3.2: The histogram shows the number of galaxies in 50 equally spaced distance bins; the dashed line is $n(r_s)$ corresponding to the Saunders selection function; the solid line is the $n(r_s)$ predicted from our derived selection function. The error bars correspond to a 14% error.

number of expansion coefficients and how the elements of the matrix W are computed. In section 3.3 we go into details of the SVD, and in section 3.4 we will describe how the linear regularisation technique is applied to find the expansion coefficients and error estimates of the reconstructed density field. Finally, in section 3.5 we summarise the whole applied procedure.

3.1 Finding the Selection Function

To perform the K-correction we need to specify the SED of the IRAS galaxies. According to [Saunders et al. 1990] and [Springel and White 1998] it can be approximated by a power law $f(\nu) \propto \nu^{-\beta}$ with $\beta = 2$. Although there might be better ways to model the SED, the power law has the advantage that calculation of the K-correction is straightforward and so it is a good compromise.

To avoid problems caused by discretisation of the fluxes (and apparent magnitudes) due to binning we spread the fluxes by adding a random variable which is uniformly distributed between $[-0.005, 0.005]$. This does not introduce a larger error, because the fluxes are given with a precision of 0.01 ([Lawrence et al. 1999]).

We neglect peculiar motions for the reconstruction of the selection function, that is, we assume $\phi(r) = \phi(r_s)$. This is certainly not true for a individual galaxy, but the error averages out for the whole set of galaxies.

3.1.1 Tests on Mock Catalogues

We have tested the method on several mock catalogues which were created in the following way:

To construct the mock catalogues, we start again at equation 2.26

$$dP_{\mu,M} = \frac{1}{A} h(\mu) d\mu f(M) dM \Theta(m_{lim} - m).$$

Defining $\zeta_M = F(M)/F(M_{lim}(\mu))$, changing the coordinates from M to ζ_M and integrating over ζ_M leads to

$$dP_{\mu} = \frac{1}{A} h(\mu) F(M_{lim}(\mu)) d\mu \quad \text{with} \quad M_{lim,i} = m_{lim} - \mu_i - \Delta(z_i) \quad (3.3)$$

We take the same spatial distribution for the mock catalogue that is provided by the PSCz catalogue, so we do not need to make assumptions such as a homogeneous spatial distribution. Let us assume the LF $\tilde{f}(M)$ and the related $\tilde{F}(M)$. Given a redshift z_i and therefore also μ_i from the PSCz catalogue we can compute $\tilde{F}(M_{lim,i})$. From equation 3.3 and the definition

of ζ_M it follows that a mock absolute magnitude M_i can be obtained by drawing a random variable ζ_M (which is uniformly distributed between 0 and 1) and computing

$$M_i = \tilde{F}^{-1}[\zeta_M \tilde{F}(M_{lim,i})] \quad (3.4)$$

F^{-1} denotes the inverse function of F . From this the apparent magnitude m_i is derived according to $m_i = M_i + \mu_i + \Delta(z_i)$. This gives us a mock catalogue with redshifts and apparent magnitudes.

Some tests are shown in figure 3.3. In Test 1 to Test 4 we constructed four mock catalogues in which \tilde{f} is a Gaussian Normal distribution with mean -20 and variance 1 , $N(-20, 1)$, but with different density parameters $\Omega_0 = 1, 0.5, 0.1, 2.0$ for the four catalogues. Tests 5 and 6 are for the CLF that corresponds to the selection function of [Saunders et al. 2000] (see also eqn. 4.1 and the comparison of our result to theirs) and for $\Omega = 1$.

The uncertainties in the fluxes of 0.01 translate into uncertainties in the apparent magnitude of e.g. 0.007 at $m = 14\text{mag}$ and 0.016 at $m = 15\text{mag}$. We added a Gaussian error (with zero mean and variance σ corresponding to the uncertainties) to the mock apparent magnitudes.

In Test 5 only four of the reconstructed selection functions for different realisations of the mock catalogue are shown (the grey lines are the reconstructions, the black dashed line is the original selection function). The variance σ was chosen to depend linearly on the apparent magnitude itself as $\sigma(m) = \sigma(m_{lim}) \cdot m/m_{lim}$ with $\sigma(m_{lim}) = 0.02$. In Test 6 eight of the reconstructed selection functions are shown (again the grey lines, and the black dashed line is the original), but with a constant variance in the apparent magnitude error of $\sigma = 0.02$. The reconstruction is in a good agreement with the original, the relative error between the reconstructed and the true selection function $(\phi_{rec} - \phi_{true})/\phi_{true}$ is 14% , if the uncertainty in apparent magnitude is constant (see Test 6). If the error in apparent magnitude depends linearly on the apparent magnitude (Test 5), the error in the selection function stays the same, but is slightly smaller for small distances.

In Tests 1 to 4 only one of the reconstructed CLFs is shown (here the original CLF is the grey line, and the reconstructed one the black one). In these cases the variance depends linearly on the apparent magnitude itself. The errors behave in the same way as in Tests 5 and 6. For the reconstructions we assumed $\Omega_0 = 1$ in all cases, but we find only a very small influence of the different Ω_0 s, so the error from the unknown Ω_0 in the reconstruction of the CLF of the PSCz galaxies should also be small.

In Tests 1 to 4 the large disagreement at the bright end in the CLFs is due to the small

amount of data in this region. The same reason explains the relatively large scatter in Tests 5 and 6 at small distances. The vertical dashed line in the plots of Tests 5 and 6 marks $\log(5\text{Mpc})$, the minimum distance of the included galaxies.

3.2 Applying the Expansion

3.2.1 Finding l_{max} and n_{max}

The truncation of the expansion series amounts to smoothing the density field over a length corresponding to the shortest wavelength in the basis functions used. The resolution of the angular mode Y_{lm} is approximately $\Delta\theta \sim \pi/l$ (see [Fisher et al. 1995]), which corresponds at distance D to an “absolute angular resolution” of $D\Delta\theta$. The resolution of the radial mode $j_l(k_{ln}r)$ can be estimated by $\Delta r \sim R_{max}\pi/z_{ln}$, where z_{ln} is the n^{th} zero of the spherical Bessel function $j_l(z)$. These can be approximated for $z \gg 1$ by $z_{ln} \sim \pi(n + l/2)$. Demanding that the radial resolution has a certain value, say $\Delta r \approx R_{max}/B$, then n_{max} can be estimated by

$$\begin{aligned} \frac{R_{max}}{B} &\approx R_{max} \frac{\pi}{z_{ln_{max}}} \quad \text{or} \\ n_{max} &\approx B - \frac{l}{2} \end{aligned} \quad (3.5)$$

To be “on the safe side” we can drop the second term and adopt $n_{max} = B$. For a given n_{max} one can choose a suitable l_{max} in the sense that the “absolute angular resolution” matches the radial resolution in a certain distance. This selected distance depends on the size of the volume one is interested in. If the density is to be reconstructed in a large volume, l_{max} must be much larger than n_{max} to achieve a good resolution at large distances. The resolution is also affected by the choice of R_{max} as $\Delta r \approx R_{max}/n_{max}$.

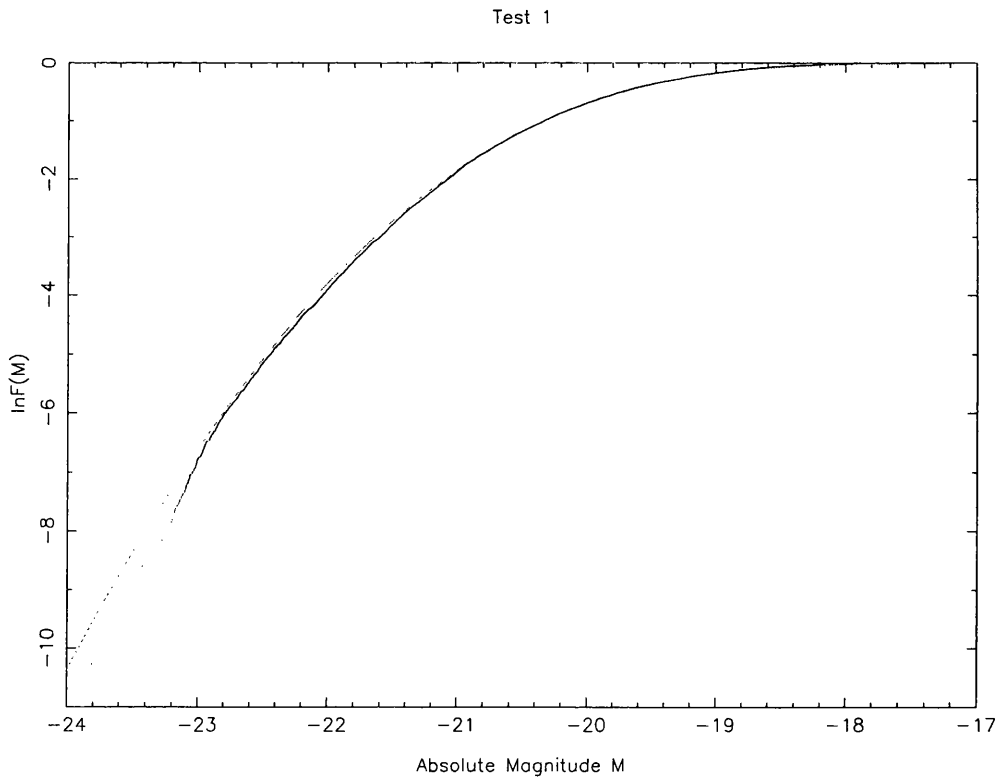
The number of used coefficients is

$$N = n_{max}(l_{max} + 1)^2. \quad (3.6)$$

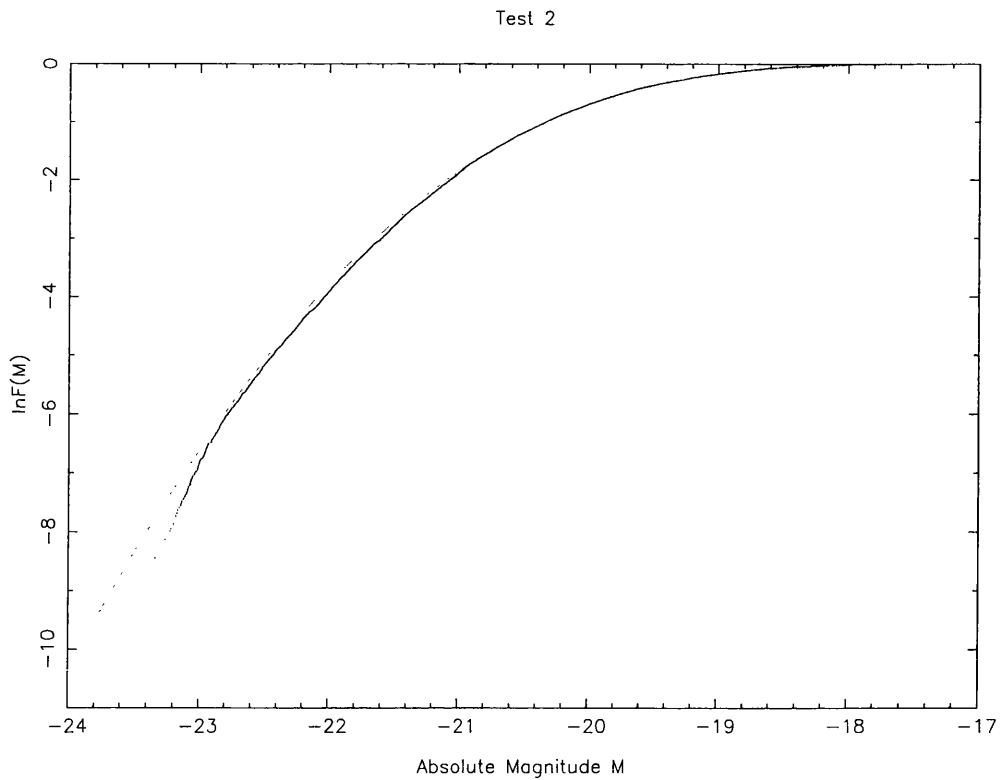
A limit for the number of coefficients used for the expansion is given by the number of data points. So N should not be larger than 10000.

As a compromise between resolution and computational effort we choose $n_{max} = 12$ and $l_{max} = 15$, which gives 3073 coefficients, a radial resolution of approx. 17Mpc and an angular resolution of about 12° . This angular resolution matches an “absolute angular resolution” of 6Mpc (17Mpc, 42Mpc) at $r = 30\text{Mpc}$ ($r = 80\text{Mpc}$, $r = 200\text{Mpc}$).

Another option is to choose a maximum wavenumber k_{max} and exclude all wavenumbers $k_{ln} > k_{max}$ as described in [Heavens and Taylor 1995] and [Tadros et al. 1999]. The n_{max}

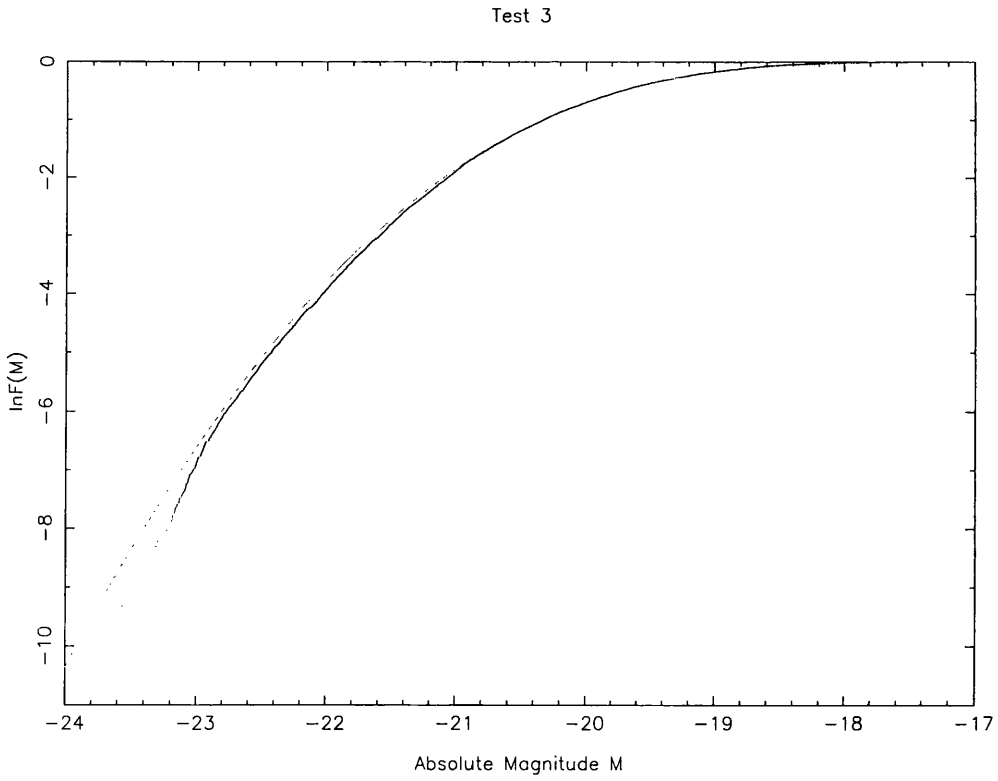


(a) Test 1

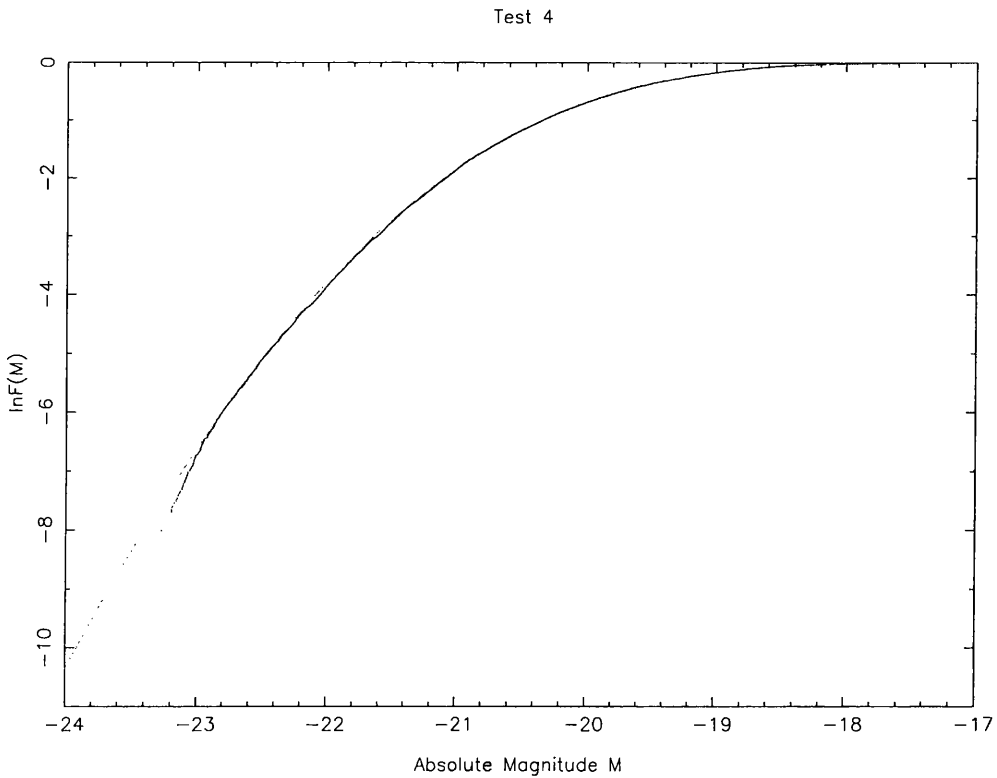


(b) Test 2

Figure 3.3: Tests of the reconstruction of the CLF and SF; see text.

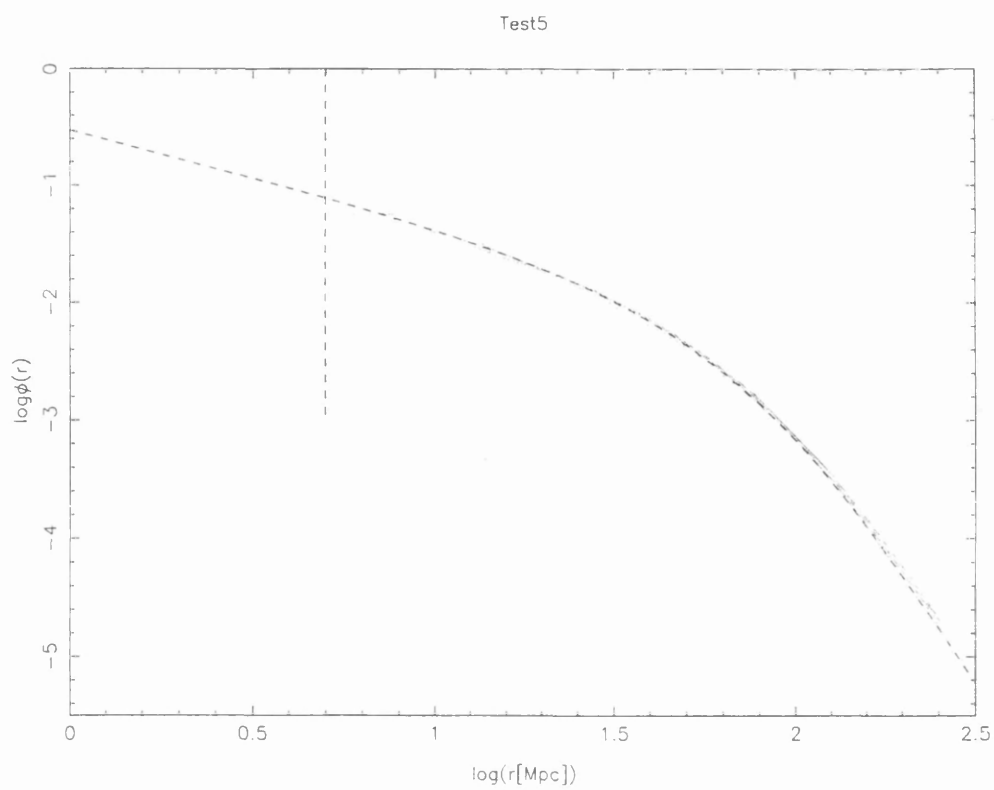


(a) Test 3

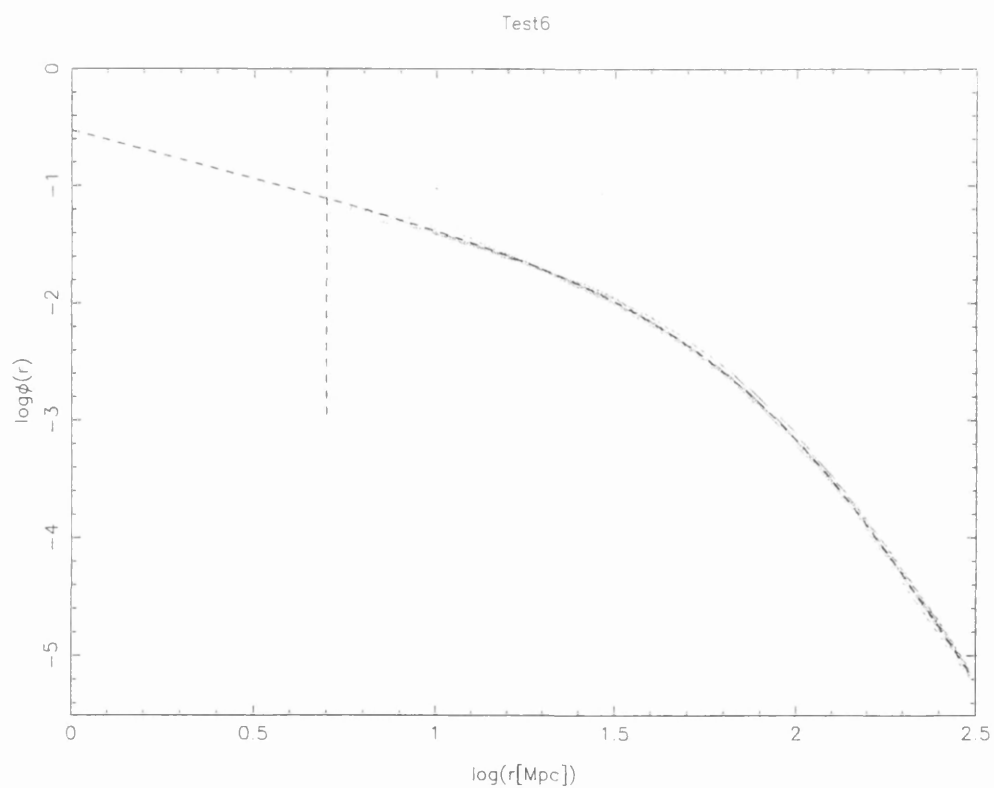


(b) Test 4

Figure 3.3 contd. Tests of the reconstruction of the CLF and SF; see text.



(c) Test 5



(d) Test 6

Figure 3.3 contd. Tests of the reconstruction of the CLF and SF; see text.

would then be dependent on l . For simplicity in the index conversion we have chosen the option with the constant n_{max} .

3.2.2 Choice of Boundary Condition

One can choose different kinds of boundary conditions (see [Fisher et al. 1995], appendix A for a detailed explanation). One option is to set the density fluctuations to zero outside the observed volume. Another is to set the fluctuations to zero only at the boundary, but this leads to an discontinuous potential and velocity field.

A third possibility is to demand that the radial peculiar velocity at the boundary vanishes. This is the same as demanding that the first derivative of the potential normal to the boundary has to vanish. The boundary is the surface of a sphere with radius R_{max} , so this boundary condition can be expressed as (see [Fisher et al. 1995], table A1; or [Tadros et al. 1999] eqn. (33))

$$\frac{d}{dr_s} j_l(k_{ln} r_s)|_{r_s=R_{max}} = 0 \quad (3.7)$$

From this relation we can find the wavenumbers k_{ln} satisfying the boundary condition.

The orthogonality relations lead to the following normalisation factors for this boundary condition (see [Heavens and Taylor 1995] eqn. (9); or [Tadros et al. 1999] eqn.(34); the two are equivalent):

$$c_{ln} = \frac{2k_{ln}^{2/3}}{\sqrt{\pi[1/4 + k_{ln}^2 R_{max}^2 - (l + 1/2)^2] J_{l+1/2}^2(k_{ln} R_{max})}} \quad (3.8)$$

This boundary condition causes the mean value of the expanded field $\rho(\vec{r})$ to be zero (see [Fisher et al. 1995]), so eqn. 2.38 has to be corrected with the mean of the density field:

$$\rho(\vec{r}_s) = \sum_{n=1}^{n_{max}} \sum_{l=0}^{l_{max}} \sum_{m=-l}^l \rho_{nlm} \cdot c_{ln} j_l(k_{ln} r_s) Y_{lm}(\theta, \varphi) + \langle \rho \rangle \quad (3.9)$$

In our short notation this reads

$$\rho(\vec{r}_s) = \sum_{i=1}^N \rho_i \Upsilon_i + \langle \rho \rangle \quad (3.10)$$

We can now define a function

$$\Upsilon_0 \equiv \frac{1}{\sqrt{V}}. \quad (3.11)$$

V is the observed volume, and the factor $1/\sqrt{V}$ normalises this function. In principle it would be possible to define this function just as $\Upsilon_0 \equiv 1$, but a Singular Value Decomposition of the matrix L (which must be inverted somehow) shows that the “zeroth” singular value is nearly

three orders of magnitude larger than the singular values if the function Υ_0 is not normalised. If it is normalised it is in the same range as the other singular values. The normalisation of this function greatly improves the numerical stability of the inversion process. Eqn. 3.10 can now be written

$$\rho(\vec{r}_s) = \sum_{i=0}^N \rho_i \Upsilon_i \quad \text{with} \quad \rho_0 \equiv \langle \rho \rangle \sqrt{V}. \quad (3.12)$$

So in every sum the summation index needs to start at zero instead of 1, and the matrices have a “zeroth” row and column. The function Ψ_0 will be a constant, and the other functions Ψ_i will be normalized to a constant.

3.2.3 Computing the Matrix Elements W_{ij}

One needs to perform the following integration to compute the elements of the matrix W :

$$\begin{aligned} W_{ij} &= \langle \Upsilon_i \Upsilon_j \rangle_{[MS]} \\ &= \int_0^{R_{max}} c_{li,ni} c_{lj,nj} j_{li}(k_{li,ni} r_s) j_{lj}(k_{lj,nj} r_s) \phi(r_s) r_s^2 dr_s \\ &\times \int_0^{2\pi} d\varphi \int_0^\pi Y_{li,mi}(\theta, \varphi) Y_{lj,mj}(\theta, \varphi) M(\theta, \varphi) \sin \theta d\theta \end{aligned} \quad (3.13)$$

We implement a Gauss-Legendre Quadrature routine with abscissas and weights from [Press et al. 1992] with 100 integration steps in the r -direction and 40 and 80 in the θ - and φ -directions, respectively. The functions Υ_i are orthonormal on the unmasked space in this approximated scalar product with an accuracy of 10^{-4} up to $l_{max} = 20$ and $n_{max} = 20$; for $l_{max} = 15$ and $n_{max} = 20$ the accuracy is 10^{-6} .

3.3 Applying SVD

To perform the SVD-inversion one has to decide which singular values need to be thrown away. It is useful therefore to look at the singular value spectrum of the matrix. Figure 3.4 shows the singular values of the matrix L for $l_{max} = 12$, $n_{max} = 15$ and $V_{max} = 20,000 \text{ km}^{-1}$ on a logarithmic scale. The condition number is approximately 4028. They are sorted in a decreasing order. We use the location of the sharp downturn in the spectrum as an indication of the most effective cutoff: a smaller cutoff will not really improve stability; a larger cutoff will give severe instability. We choose the allowed condition number to be of magnitude 27.5. The dotted part of the spectrum is excluded, these are 551 singular values. The results, however, are not sensitive to small changes in the choice of the cutoff. The allowed condition

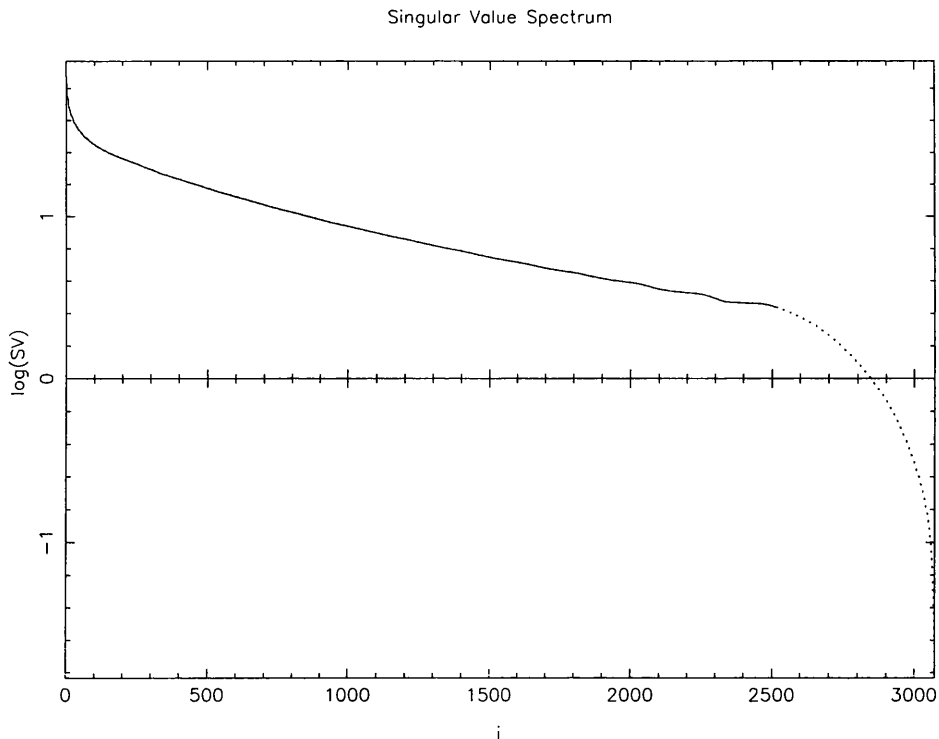


Figure 3.4: Logarithmic plot of the singular values of the matrix L , for $l_{max} = 15$ and $n_{max} = 12$. The singular values are sorted into descending order. The dotted part is excluded.

number would have to be much larger (at least a factor of 3) if the maximum redshift is chosen to be $30,000\text{kms}^{-1}$ instead of $20,000\text{kms}^{-1}$.

Another indicator for where to choose allowed condition number is the mean density, because there are two ways to compute it. On the one hand it is defined as $\langle \rho \rangle = \rho_0 / \sqrt{V}$ (see eqn. 3.12), this result will depend on the number of excluded singular values. On the other hand the mean density can be computed independently from the whole Gorski Method by eqn. 3.23. It turns out that the first way yields a much larger value than the second way if we do not exclude any singular values, and vice versa if we make the allowed condition number much smaller. The two agree very well for an allowed condition number of 27.5.

Because the matrix L is a lower triangular one, in theory its inverse would be a lower triangular matrix, too. However, some of the singular values are thrown away, so the “modified” inverse $L_M^{-1} = V \cdot W_M^{-1} \cdot U^T$ (with the modified matrix W_M , in which the reciprocals of the small singular values are replaced by zero) will not be a lower triangular matrix.

To replace the reciprocals of some singular values by zero does not mean to exclude some basis functions. A closer look at what happens when $V \cdot W_M^{-1} \cdot U^T$ is computed shows that the zeros on the diagonal of W_M^{-1} generate some blank rows in $W_M^{-1} \cdot U^T$ (or blank columns in $V \cdot W_M^{-1}$), but this does not necessarily generate blank rows or columns in $V \cdot W_M^{-1} \cdot U^T$.

3.4 Computation of Coefficients by Linear Regularisation, Error Estimation

Let us call the the coefficients of the functions Ψ_j (the ones that are orthonormal on the masked space) R_j so that the density is expressed in this basis as

$$\rho(\vec{r}_s) = \sum_j R_j \Psi_j. \quad (3.14)$$

In principle the coefficients R_j can be computed by

$$R_j = \langle \rho, \Psi_j \rangle_{[MS]} \quad (3.15)$$

where we have already mentioned that we can approximate the scalar product by a sum over all galaxies in the catalogue (see eqn. 2.47). This is the step where we introduce shot noise, because we are replacing a (continuous) integral by a (discrete) sum, as we are going from a continuous field to a finite dataset. The sum will not be exactly the integral but

$$\begin{aligned} R_{j,raw} &\equiv \sum_{\text{galaxies}} \Psi_j(\vec{r}_{\text{galaxy}}) = \langle \rho, \Psi_j \rangle_{[MS]} + \sigma_j \quad \text{or} \\ R_{j,raw} &= R_j + \sigma_j, \end{aligned} \quad (3.16)$$

where σ_j is the shot noise of the coefficient $R_{j,raw}$. Because these are the coefficients of the orthonormal basis on the masked space, their errors are uncorrelated, the covariance matrix is diagonal. The sum can be seen as a sum over all galaxies with a certain weight applied to each galaxy. Therefore the error of this sum σ_j can be estimated by the generalisation of the Poissonian error with unequal weighting (see [Yahil et al. 1991]).

$$\sigma_j = R_j \cdot \frac{\sqrt{\sum_{\text{galaxies}} |\Psi_j(\vec{r}_{\text{galaxy}})|^2}}{\sum_{\text{galaxies}} |\Psi_j(\vec{r}_{\text{galaxy}})|} \quad (3.17)$$

Because the covariance matrix is diagonal the χ^2 measure simplifies to

$$\chi^2 = \sum_j \frac{(\hat{R}_j - R_j)^2}{\sigma_j^2} \quad (3.18)$$

To find a measure of smoothness Ξ we assume that the density field $\rho(\vec{r})$ is not too different from a constant B (which is obviously the mean density). The expansion of a constant field in our SH&SB is straightforward to compute, let the coefficients be B_i . According to the definitions of the matrix L one can transform the coefficients of the SH&SB to the coefficients of the Ψ_j by

$$b_j = \sum_i L_{ji}^T B_i \quad \text{so that } \rho = B = \sum_j b_j \Psi_j. \quad (3.19)$$

A positive functional that is a measure of smoothness of ρ is

$$\Xi = \sum_j (\hat{R}_j - b_j)^2 \quad (3.20)$$

This functional will be minimal (equal to zero) if the estimators of the coefficients \hat{R}_j are equal to the expansion coefficients of the constant field B , that means if the estimated density equals constant B . This formalism can also be applied to other expected density fields, then the coefficients B_i and b_j for this density need to be computed.

If we now minimise $\chi^2 + \lambda\Xi$ according to inverse problem theory we obtain $N + 1$ equations from

$$\frac{\partial}{\partial \hat{R}_j} (\chi^2 + \lambda\Xi) = 0 \quad \text{for } j = 0, \dots, N \quad (3.21)$$

Computing the derivatives leads to $N + 1$ equations

$$\hat{R}_j = \frac{1}{\lambda\sigma_j^2 + 1} R_{j,raw} + \frac{\lambda\sigma_j^2}{\lambda\sigma_j^2 + 1} b_j \quad (3.22)$$

Things do even become easier as only the coefficient B_0 is different from zero. By definition $B_0 = \langle \rho \rangle \sqrt{V} = B\sqrt{V}$. Also only b_0 is different from zero because the transformation matrix between \vec{B} and \vec{b} is a upper triangular matrix, so $b_0 = L_{00}^T \cdot B\sqrt{V} = L_{00} \cdot B\sqrt{V}$. Now we only need to compute the mean density, as $B = \langle \rho \rangle$. It can be found using

$$\langle \rho \rangle = \frac{1}{V_{\text{observed}}} \sum_{\text{galaxies}} \frac{1}{\phi(r_{\text{galaxy}})} \quad (3.23)$$

The error in the mean density is computed analogously to eqn. 3.17:

$$\begin{aligned} \Delta \langle \rho \rangle &= \langle \rho \rangle \cdot \frac{\sqrt{\sum_{\text{galaxies}} |1/\phi(r_{\text{galaxy}})|^2}}{\sum_{\text{galaxies}} |1/\phi(r_{\text{galaxy}})|} \\ &= \frac{1}{V_{\text{observed}}} \sqrt{\sum_{\text{galaxies}} |1/\phi(r_{\text{galaxy}})|^2} \end{aligned} \quad (3.24)$$

Now we can compute the estimates for the coefficients \hat{R}_j :

$$\hat{R}_0 = \frac{1}{\lambda\sigma_0^2 + 1} R_{0,raw} + \frac{\lambda\sigma_0^2}{\lambda\sigma_0^2 + 1} L_{00} \cdot \langle \rho \rangle \sqrt{V} \quad \text{and} \quad (3.25)$$

$$\hat{R}_j = \frac{1}{\lambda\sigma_j^2 + 1} R_{j,raw} \quad \text{for } j = 1, \dots, N \quad (3.26)$$

The linear regularisation will effect that the zeroth coefficient is corrected towards the expected mean density and the other coefficients are more and more suppressed as λ grows. Therefore the fluctuations in the density field will be decreased, and in the extreme case of $\lambda \rightarrow \infty$ the density will be constant.

We have to find the amount of regularisation we need for our problem. A reasonable choice for λ would make the residuals $|\hat{R}_i - R_{i,raw}|$ to be of the same size as the expected errors σ_i . So the criterion for the ‘‘compromise parameter’’ λ is

$$\sum_{j=0}^N (\hat{R}_j - R_{j,raw})^2 \approx \sum_j \sigma_j^2 \quad (3.27)$$

It turns out that the amount of regularisation we have to apply is not very large. This can be expected as we have already applied the SVD for the inversion, and as the result should not depend too much on the a priori assumption.

As we already mentioned, the coefficients of the orthonormalised functions and their errors are independent. Thus, to work in the orthonormal basis provides an easy method to estimate the errors on the reconstructed density, because the density in a certain point is a sum over independent variables, which means that the errors add in quadrature:

$$\Delta\rho(\vec{r}_s) = \sqrt{\sum_j (\hat{\sigma}_j \Psi_j(\vec{r}_s))^2} \quad (3.28)$$

Of course we have to use the errors $\hat{\sigma}_j$ of the estimated coefficients \hat{R}_j . These can be found from the from eqn. 3.26:

$$\hat{\sigma}_0^2 = \left(\frac{1}{\lambda\sigma_0^2 + 1}\sigma_0\right)^2 + \left(\frac{\lambda\sigma_0^2}{\lambda\sigma_0^2 + 1}L_{00} \cdot \Delta \langle \rho \rangle \sqrt{V}\right)^2 \quad \text{and} \quad (3.29)$$

$$\hat{\sigma}_j = \frac{1}{\lambda\sigma_j^2 + 1}\sigma_j \quad \text{for } j = 1, \dots, N \quad (3.30)$$

The errors of the coefficients of the SH&SB can be found by analogy with eqn. 3.28, because these coefficients are a linear combination of independent variables, too.

$$\Delta\rho_i = \sqrt{\sum_j (L_{ij}^{-1T} \hat{\sigma}_j)^2} \quad (3.31)$$

We excluded from the reconstruction all the modes where the relative error of the coefficient was larger than 10%: $\Delta\rho_i/\rho_i > 0.1$. We also reconstructed the density with all modes and did not find a visible difference. This is caused by the coefficients with large relative errors being very small themselves and so not contributing to the density.

3.5 The Applied Procedure summarised

Below we summarise the most important steps of the whole applied method in keywords.

- Convert fluxes to apparent magnitudes
- Convert heliocentric redshifts to CMB-redshifts
- Translate redshifts z into redshift distances r_s (eqn. 3.2)

Selection Function

- Spread the measured fluxes to avoid problems that can be caused by the discretisation of the fluxes
- Follow steps in section 2.6 with $\beta = 2$

Density Reconstruction

- Mean density: $\langle \rho \rangle = \frac{1}{V_{obs}} \sum_{galaxies} 1/\phi(r_s)$, (is from SF only)
error of the mean density: $\Delta \langle \rho \rangle = \frac{1}{V_{obs}} \sqrt{\sum_{galaxies} |1/\phi(r_{galaxy})|^2}$
- Define $\Upsilon_0 \equiv 1/\sqrt{V}$ and $\rho_0 \equiv \sqrt{V} \langle \rho \rangle$
- Select maximum redshift V_{max}
- Select l_{max} and n_{max} ; the number of modes is $N + 1 = n_{max}(l_{max} + 1)^2 + 1$; the absolute angular resolution in distance D is $D \cdot \pi/l_{max}$, the radial resolution is R_{max}/n_{max}
- Find wavenumbers k_{ln} from: $\frac{d}{dr_s} j_l(k_{ln} r_s)|_{r_s=R_{max}} = 0$;
and normalisation constants $c_{ln} = 2k_{ln}^{2/3} / \sqrt{\pi[1/4 + k_{ln}^2 R_{max}^2 - (l + 1/2)^2] J_{l+1/2}^2(k_{ln} R_{max})}$
- Compute W_{ij} for $i = 0, \dots, N$; $j = i, \dots, N$ (see eqn. 3.13; upper triangle is enough, as W is symmetric)
- Find L by Choleski-decomposition of W
- Perform Singular Value Inversion of L with an allowed condition number picked from a plot of the singular values and $\langle \rho \rangle_{from SF only} \approx \rho_0/\sqrt{V}$
- Construct new set of functions: $\Psi_j = \sum_i L_{ji}^{-1} \Upsilon_i$

- Find raw coefficients $R_{j,raw} = \sum_{\text{galaxies}} \Psi_j(\vec{r}_{\text{galaxy}})$
and $\sigma_j = R_j \cdot \frac{\sqrt{\sum_{\text{galaxies}} |\Psi_j(\vec{r}_{\text{galaxy}})|^2}}{\sum_{\text{galaxies}} |\Psi_j(\vec{r}_{\text{galaxy}})|}$ for $j = 0, \dots, N$
- With the assumption that the density is not too different from a constant the estimators for the coefficients \hat{R}_j become:
 $\hat{R}_0 = \frac{1}{\lambda\sigma_0^2+1} R_{0,raw} + \frac{\lambda\sigma_0^2}{\lambda\sigma_0^2+1} L_{00} \cdot \langle \rho \rangle \sqrt{V}$ and
 $\hat{R}_j = \frac{1}{\lambda\sigma_j^2+1} R_{j,raw}$ for $j = 1, \dots, N$;
and their errors $\hat{\sigma}_j$:
 $\hat{\sigma}_0^2 = (\frac{1}{\lambda\sigma_0^2+1} \sigma_0)^2 + (\frac{\lambda\sigma_0^2}{\lambda\sigma_0^2+1} L_{00} \cdot \Delta \langle \rho \rangle \sqrt{V})^2$ and
 $\hat{\sigma}_j = \frac{1}{\lambda\sigma_j^2+1} \sigma_j$ for $j = 1, \dots, N$;
select λ so that $\sum_{j=0}^N (\hat{R}_j - R_{j,raw})^2 \approx \sum_j \sigma_j^2$
- $\hat{\rho}_i = \sum_{j=0}^N L_{ij}^{-1T} \hat{R}_j$
- Reconstruct density $\rho(\vec{r}_s) = \sum_{i=0}^N \hat{\rho}_i \Upsilon_i(\vec{r}_s)$,
(exclude all ρ_i with $\Delta\rho_i/\rho_i > 0.1$)
the errors and the density are $\Delta\rho(\vec{r}_s) = \sqrt{\sum_j (\hat{\sigma}_j \Psi_j(\vec{r}_s))^2}$

List of Parameters

Minimum Redshift (CMB frame):	$cz_{min} = 500\text{kms}^{-1}$
Maximum Redshift:	$cz_{max} = 20,000\text{kms}^{-1}$
number of included galaxies:	$N_{gal} = 10654$
Number of Modes:	$n_{max} = 12$
	$l_{max} = 15$
Total number of modes:	$N + 1 = 3073$
angular resolution:	$\Delta\theta = 12^\circ$
angular resolution in $D = 80\text{Mpc}$:	$D \cdot \Delta\theta = 17\text{Mpc}$
radial resolution:	$\Delta r = 17\text{Mpc}$
allowed condition number:	27.5
limiting apparent magnitude:	$m_{lim} = 15.0731$
SED exponent:	$\beta = 2$
Hubble Constant:	$H_0 = 100h^{-1}\text{kms}^{-1}\text{Mpc}^{-1}$
Density Parameter	$\Omega_0 = 1$

Chapter 4

Results and Discussion

4.1 Selection Function

The CLF of the PSCz galaxies is shown in figure 4.1, and the selection function $\phi(r)$ in figure 4.2. As we already mentioned, the selection function and the CLF are reconstructed up to the normalising constant, but this unknown constant cancels in the overdensity.

[Saunders et al. 2000] give the selection function as

$$\phi(r) = \phi_* \left(\frac{r}{r_*}\right)^{1-\alpha} \left[1 + \left(\frac{r}{r_*}\right)^\gamma\right]^{-\frac{\beta}{\gamma}} \quad (4.1)$$

with $\phi_* = 0.0077$, $\alpha = 1.82$, $r_* = 86.4$, $\gamma = 1.56$, $\beta = 4.43$.

In figure 4.2 we compare this with the selection function we derive. The Saunders-selection function is shown as a grey line, our result as a black line. The lower black line is our SF when we include K-correction and use the luminosity distance, the upper one when we do not perform the K-correction and take $r = cz/H_0$.

Up to 100Mpc the relative difference $(\phi_{our} - \phi_{Saunders})/\phi_{Saunders}$ between our reconstructed SF and the Saunders-SF is less than 10%, this is also the relative error given by [Saunders et al. 2000]. At 200Mpc the relative difference between our corrected version (uncorrected version) and the Saunders-SF increases to 23% (13%), and at 300Mpc to 31% (18%). The difference between our corrected and uncorrected versions is visible beyond 100Mpc. At lower distances the agreement between the two selection functions is good, but at distances of more than 100Mpc our selection function is significantly steeper.

A selection function corresponds to a function $n(r_s)$ where $n(r_s)dr_s \propto \rho > 4\pi r_s^2 \phi(r_s)dr_s$ is a prediction of the number of observed galaxies with distances between r_s and $r_s + dr_s$ (in the case of a homogeneous density). Figure 3.2 shows the $n(r_s)$ that corresponds to our selection function (the solid line), and the one that corresponds to the Saunders selection function (the

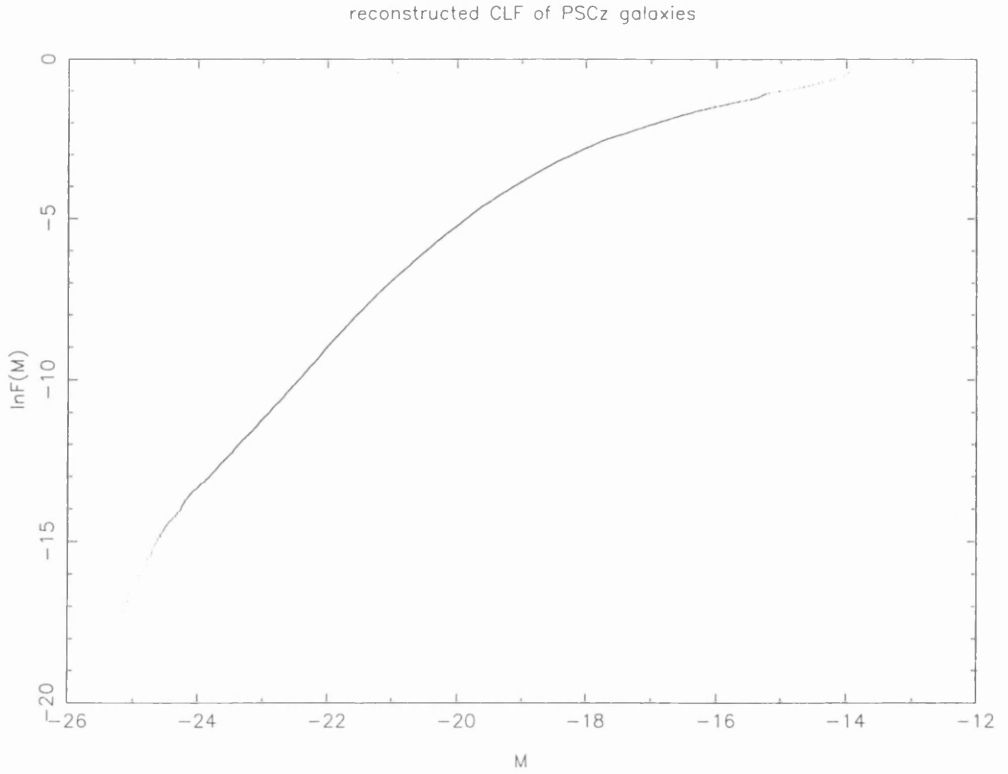


Figure 4.1: Reconstructed CLF of the PSCz catalogue (the normalisation is arbitrary).

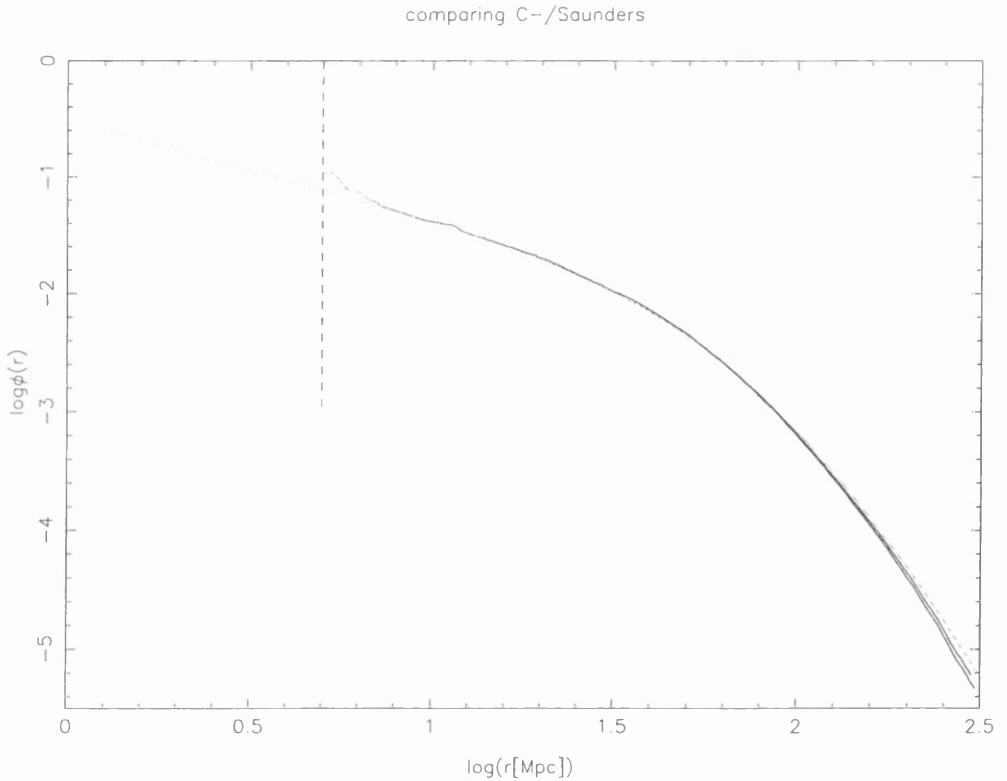


Figure 4.2: Comparison of our SF (black line) with that of [Saunders et al. 2000] (grey line); lower black line is our SF with K-correction and $r = d_L$, the upper one is without K-correction and with $r = cz/H_0$; dashed line marks $\log(5Mpc)$.

dashed line), the histogram shows the number of PSCz galaxies in certain distance bins. The error bars attached to our selection function are 14% errors, as determined from the mock catalogues. It seems that the Saunders selection function can describe the data better over a larger distance range, whereas our selection function seems to be too steep. But up to $r_s = 200\text{Mpc}$ the two functions and the data agree within the error bars.

We tested the influence of the selection function and also reconstructed the density with the Saunders SF. Figures 4.7 and 4.8 show these results. There are no large differences to the reconstruction with our selection function (see figures 4.3 and 4.4), the overdensities and voids are in the same positions, but in the reconstruction with the Saunders selection function the peaks are slightly higher. As the selection function only tells us how to rescale the observed peaks (recall the definition of the selection function), a change in the selection function should affect mainly the height of the peaks but not their position.

4.2 A Cosmographical Tour

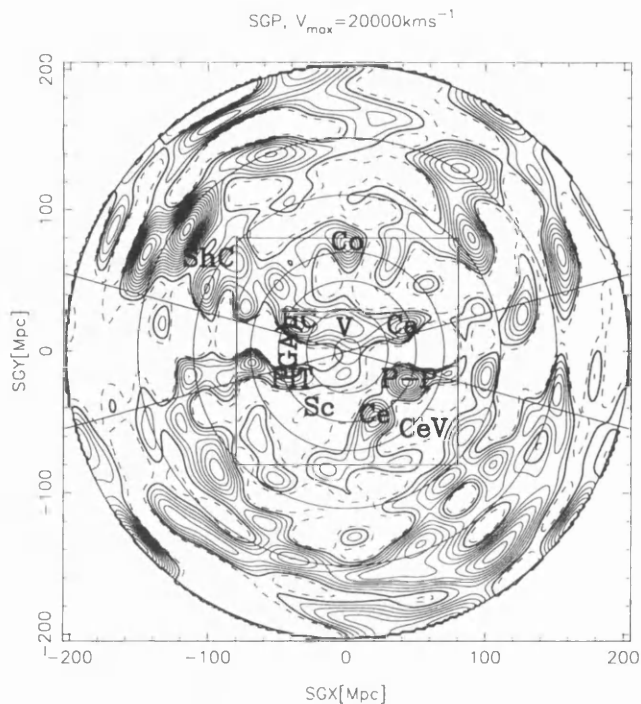
Figures 4.3 and 4.4 show the results of the reconstruction of the overdensity field in redshift space.

Figure 4.3 shows contour plots of the overdensity field in the Supergalactic Plane (SGP). The x-axis of this plane points towards the galactic coordinates $(l, b) = (137.37^\circ, 0^\circ)$, the y-axis towards $(l, b) = (227.37^\circ, 83.68^\circ)$. The second subfigure is a clipping of the first, the clipped area is marked in the first by the rectangle. The contour lines are spaced at $\Delta\delta = 0.5$, and the heavy solid line marks $\delta = 0$ (the mean density); solid lines are overdensities and dashed lines underdensities. The region close to the x-axis between the two straight lines is in reality covered by the mask.

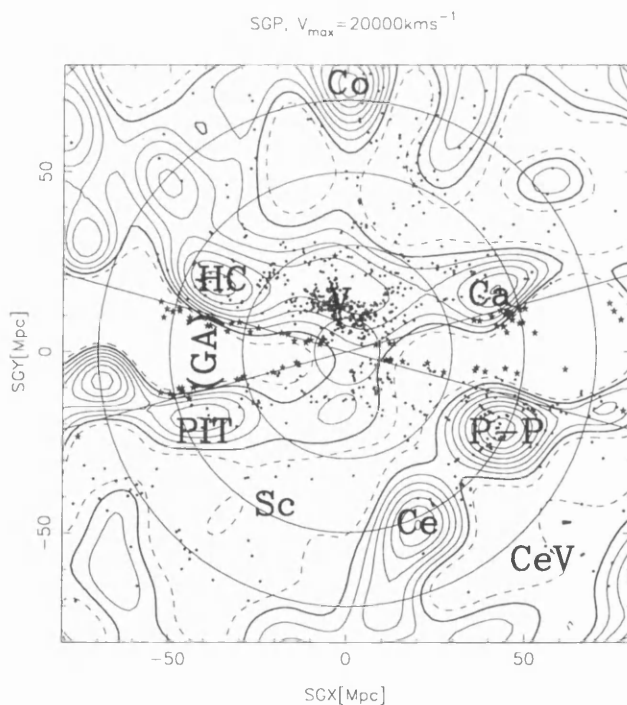
Figure 4.4 shows maps of the overdensity in spherical shells with different radii, we are at the centre of these shells. We used an Aitoff projection of the galactic coordinates (l, b) , the galactic centre is in the centre of the plot. The grey shaded areas at and near $b = 0^\circ$ denote the masked regions. The colours code the density, they are also spaced at $\Delta\delta = 0.5$. The line between green and light blue marks the $\delta = 0$ contour. The density grows from green \rightarrow yellow \rightarrow orange \rightarrow red \rightarrow pink \rightarrow dark red, and drops over light blue and light lilac. In the shell plots the SGP is marked by the heavy black line, the directions of the x- and y-axis of the SGP are indicated by a cross, and the inverse directions by the open circles.

The light concentric circles in figure 4.3 show the radii of the shells.

In both figures the black dots are the galaxies in the shell/SGP (within a distance of less

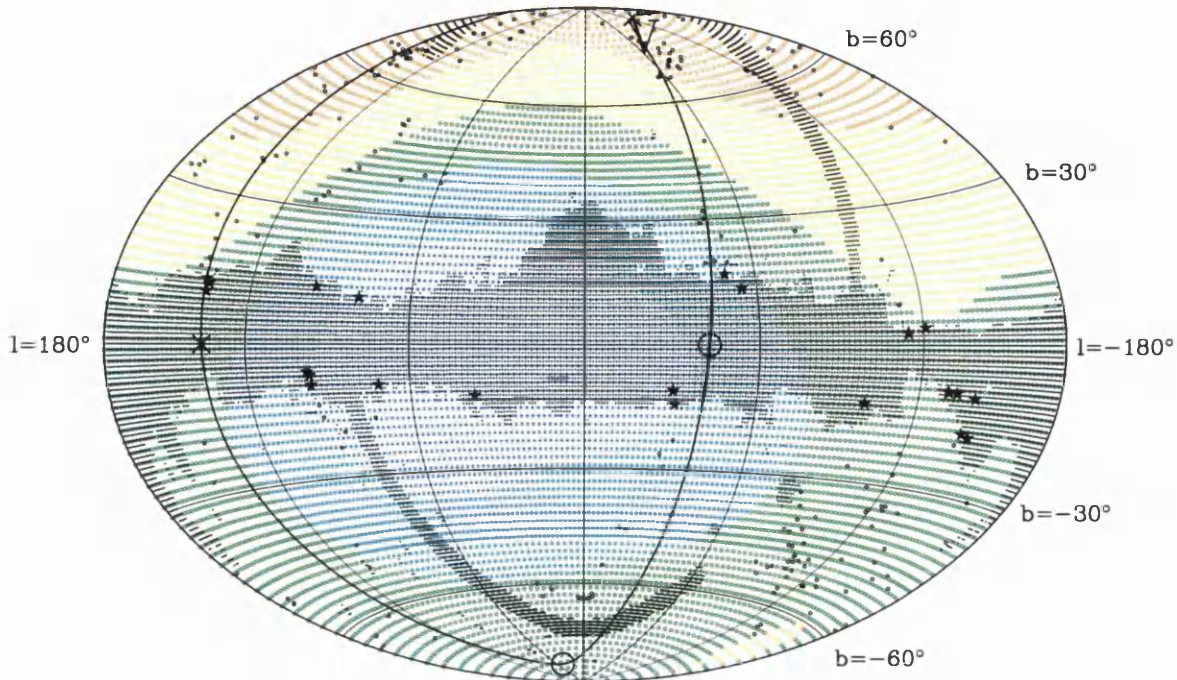


(a) Density Field in SGP

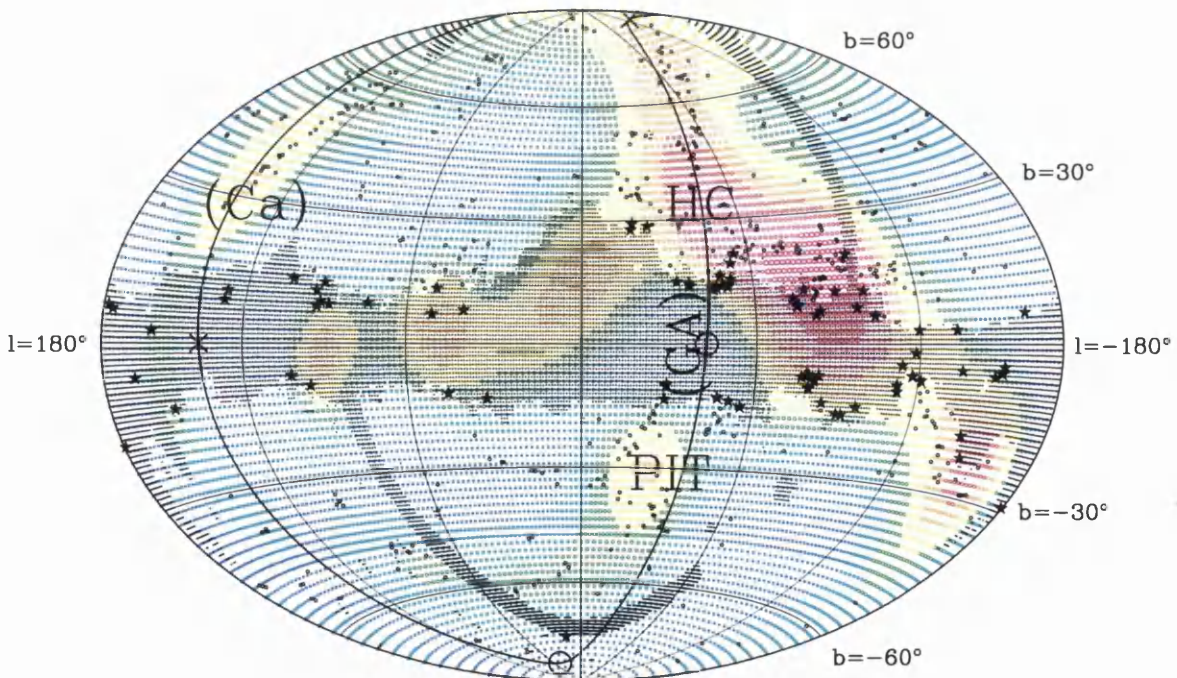


(b) Density Field in SGP; clipping from previous figure

Figure 4.3: Reconstructed density field (with $V_{max} = 20,000\text{kms}^{-1}$) in the Supergalactic plane and galaxies with $|SGZ| < 3\text{Mpc}$; contours are at $\Delta\delta = 0.5$; see also text.

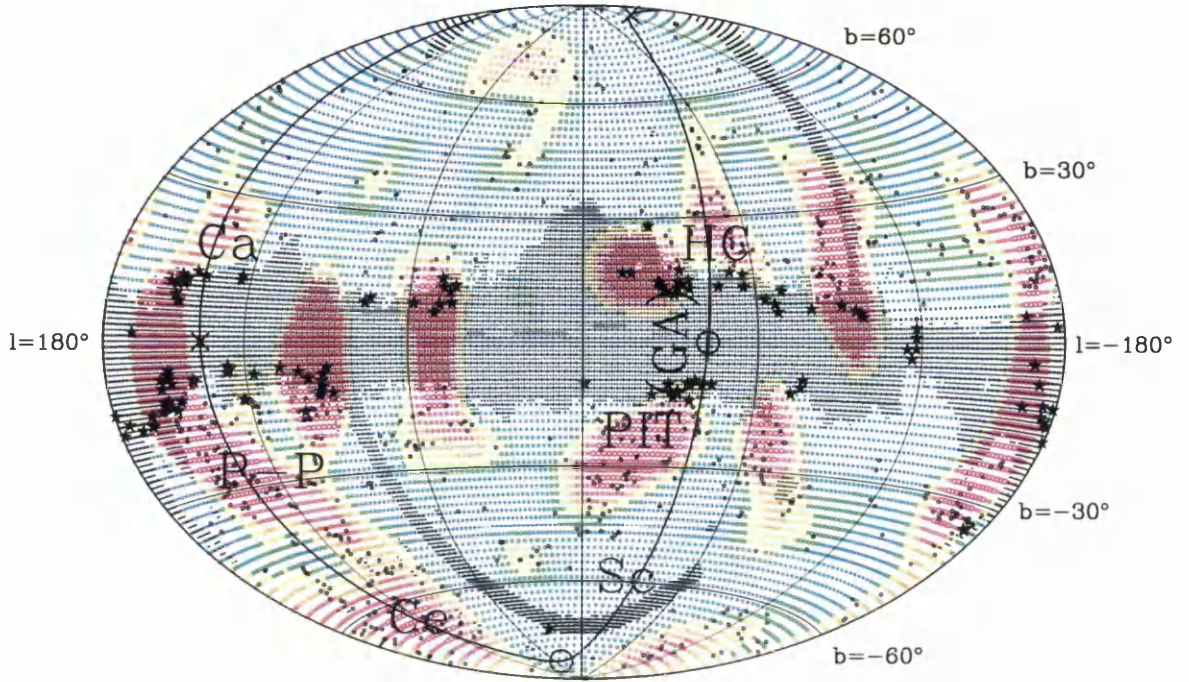


(a) Density in shell $r_s = 10\text{Mpc}$

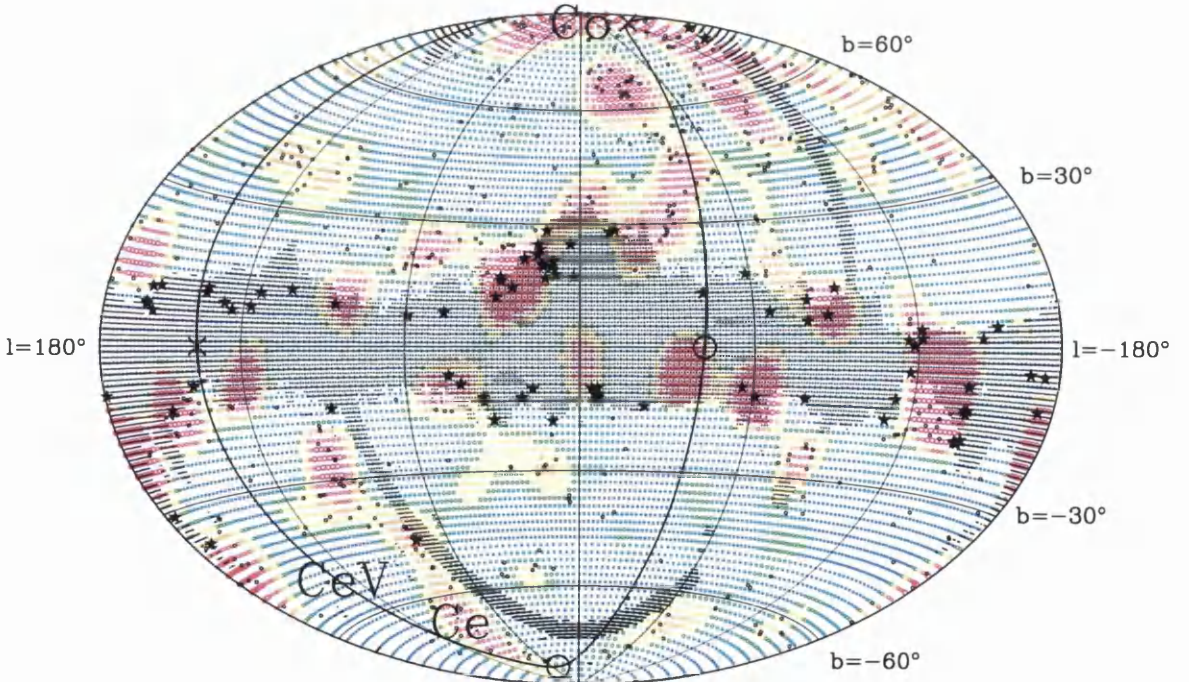


(b) Density in shell $r_s = 30\text{Mpc}$

Figure 4.4: Reconstructed density field in shells with radius r_{shell} , and galaxies with $r_s = r_{shell} \pm 3\text{Mpc}$; see also text.



(a) Density in shell $r_s = 50\text{Mpc}$



(b) Density in shell $r_s = 70\text{Mpc}$

Figure 4.4 contd: Reconstructed density field in shells with radius r_{shell} , and galaxies with $r_s = r_{shell} \pm 3\text{Mpc}$; see also text.

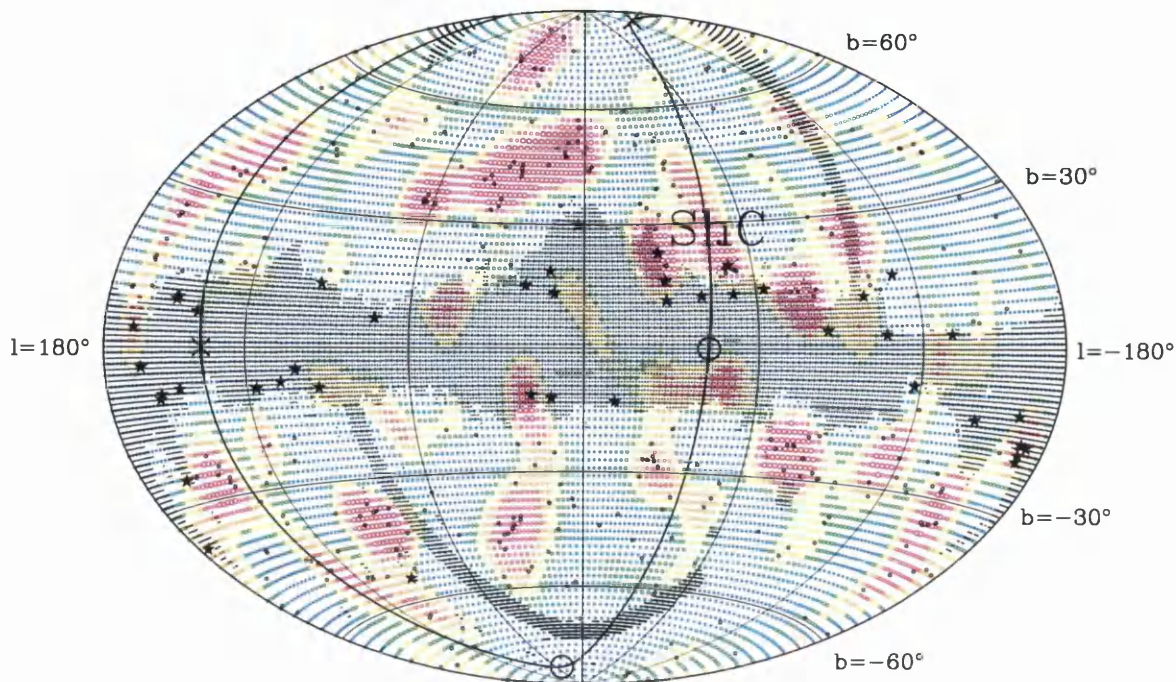
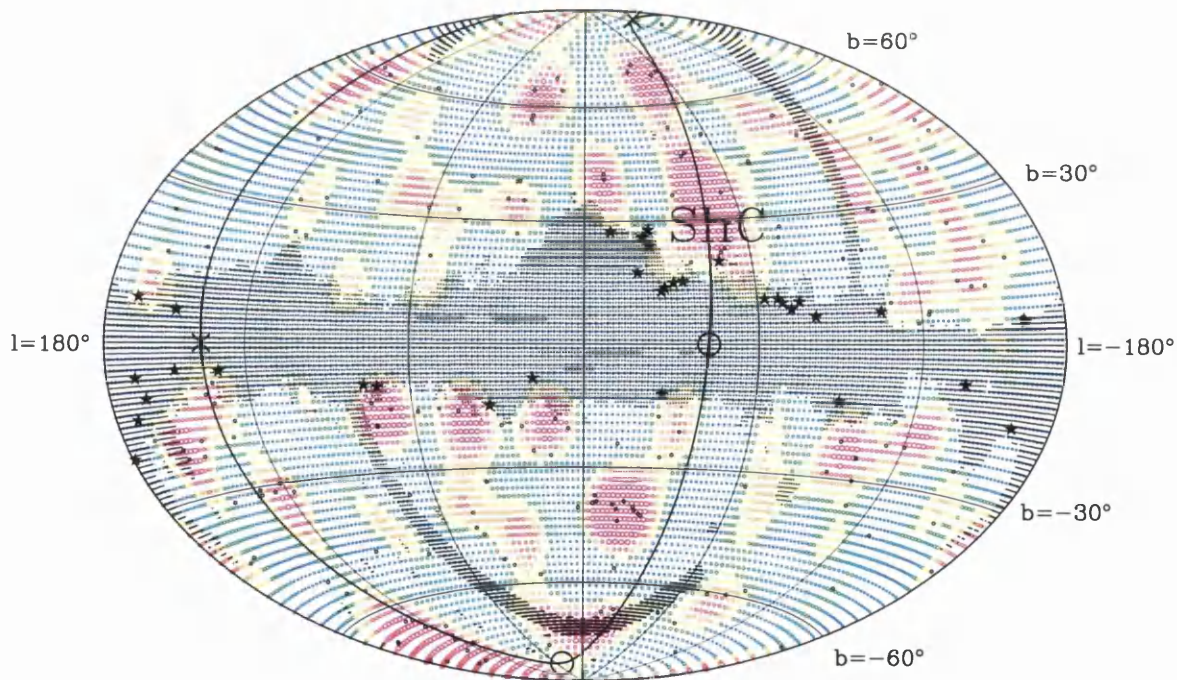
(c) Density in shell $r_s = 110\text{Mpc}$ (d) Density in shell $r_s = 150\text{Mpc}$

Figure 4.4 contd: Reconstructed density field in shells with radius r_{shell} , and galaxies with $r_s = r_{shell} \pm 3\text{Mpc}$; see also text.

than 3Mpc from the shell/SGP). The small stars mark the galaxies of the PSCz catalogue which are behind the bigger mask and so were never used during the analysis.

Prominent structures are labelled (names are taken from [Strauss and Willick 1995] and [Teodoro 1999]):

HC	=	Hydra-Centaurus supercluster
PIT	=	Pavo-Indus-Telescopium supercluster
GA	=	Great Attractor
V	=	Virgo cluster
P-P	=	Perseus-Pisces supercluster
Ca	=	Camelopardalis supercluster
Ce	=	Cetus Wall
Co	=	Coma-A1367 Supercluster
ShC	=	Shapeley Concentration
Sc	=	Sculptor Void
CeV	=	void behind the Cetus Wall.

4.2.1 Behind the Mask

The Gorski Method only uses information from the unmasked regions, and in fact it “extracts” from the usual SH&SB basis the part that describes the unmasked region. Similar to the range and the nullspace of a singular matrix the new basis describes the “range of the data” without pollution by the “nullspace of the data” (which are the masked regions), leaving this behind. Hence the reconstructed field is only reliable in the unmasked regions.

Because we use a certain resolution we assume a minimum size for structures, and the reconstruction can sometimes interpolate successfully into the mask up to distances corresponding to the resolution. If the mask is smaller than the resolution, interpolation over the mask may also work. An example of both cases can be seen in in the shell with $r = 50\text{Mpc}$: the connection between the Camelopardalis supercluster and the Perseus-Pisces supercluster is made, also the overdensities at $l = 190^\circ = -170^\circ$ are connected, but the Hydra-Centaurus and Pavo-Indus-Telescopium supercluster were not connected, although the unused galaxies (marked by the small stars) suggest they should be. Also in recent literature (e.g. [Strauss and Willick 1995], [Teodoro 1999], and [Fisher et al. 1995]) these two clusters are usually connected and named the Great Attractor, but in this region the mask is signifi-

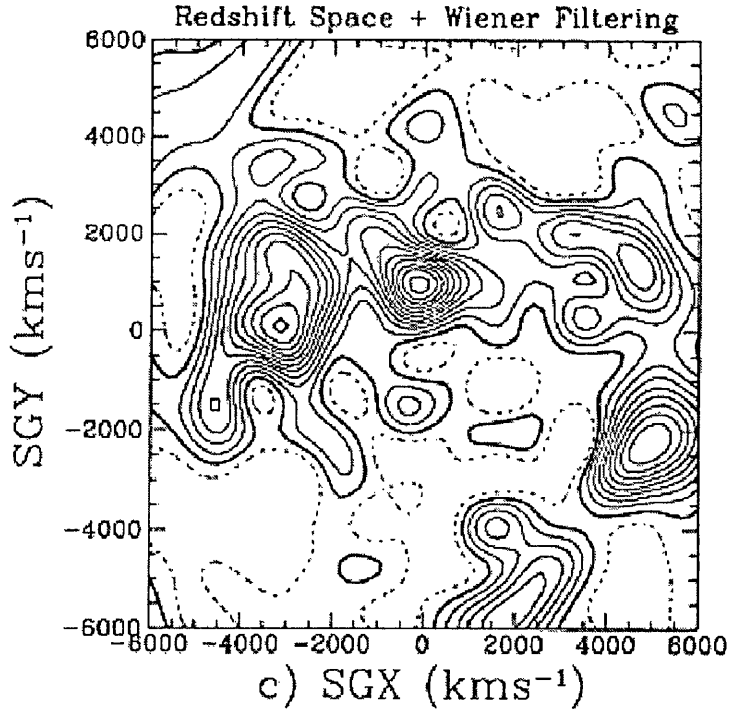


Figure 4.5: Reconstructed density field in the Supergalactic plane up to distances of 60Mpc, contour lines at $\Delta\delta = 0.5$, from [Fisher et al. 1995].

cantly larger than our smoothing length.

4.2.2 Discussion

At small and medium distances and outside the mask the density maps show a good agreement with the data -the distribution of the PSCz galaxies-, as well as with overdensity maps derived by other methods (e.g. overdensity maps in the SGP from [Fisher et al. 1995], [Teodoro 1999] and [Strauss and Willick 1995]). All prominent structures can be easily identified. Some differences may be expected as our maps are in redshift space, while some of the above references give real space maps. One important difference between the maps in real space and redshift space is that the amplitude of the overdensity fluctuations is smaller in real space, this can be seen when our maps are compared to real space maps. In [Fisher et al. 1995] there is also a map in redshift space (in the SGP, it is given here in figure 4.5), and the corresponding peaks in the overdensity in this map agree well with the ones in our map in position and in amplitude.

We also reconstructed the density field for a different maximum redshift and truncation in the expansion. Figure 4.6 shows the result for $V_{max} = 25,000\text{kms}^{-1}$, $n_{max} = 15$, and

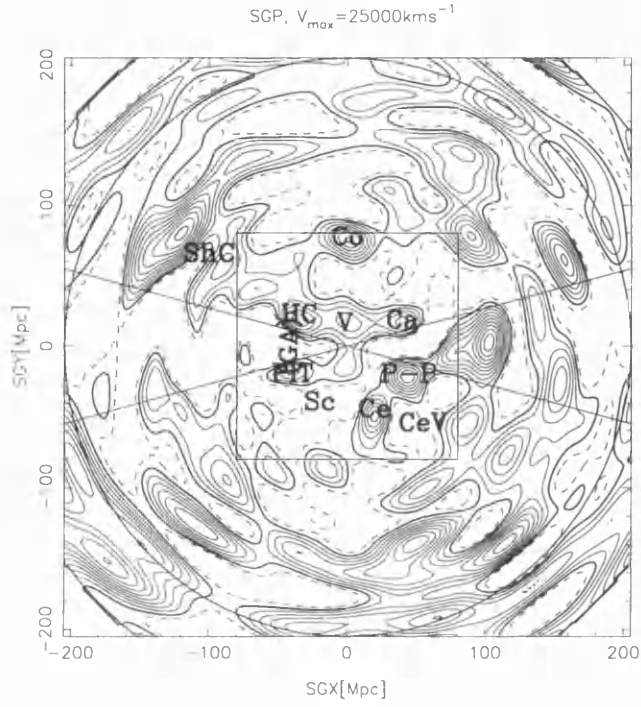
$l_{max} = 12$. One can see the effect of the lower angular resolution (15° instead of 12°), but otherwise we do not find the result sensitive to these changes.

If one looks at the SGP map at larger distances ($r > 150\text{Mpc}$) structures seem to be arranged “in shells” around us. This is an artefact that arises due to the constant angular resolution and the constant radial resolution. As the resolved angle stays constant the “absolute angular resolution” increases with distance, whereas the “absolute radial resolution” remains constant. We matched the absolute radial and angular resolution at a distance of $r = 80\text{Mpc}$. The effect is then not too strong up to distances of 150Mpc , where the absolute angular resolution is twice the radial resolution. This shell behaviour could be avoided by choosing n_{max} dependent on l as mentioned in section 3.2.1.

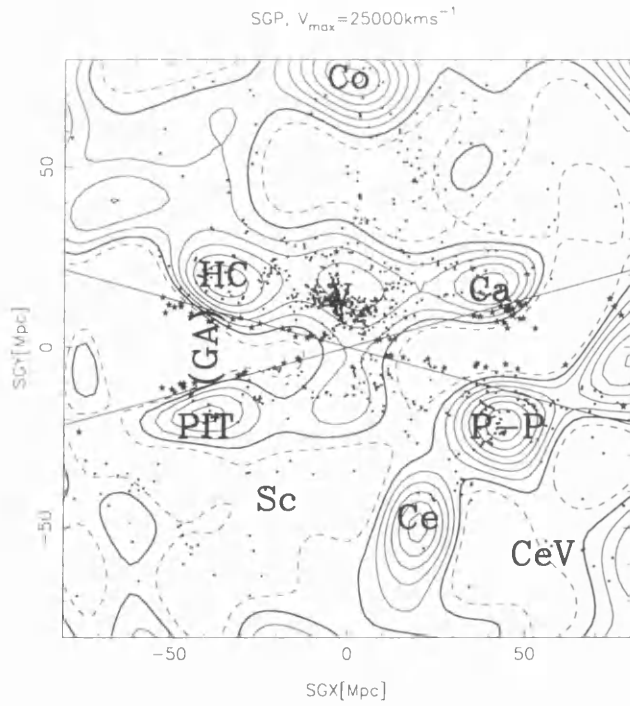
Figures 4.7 and 4.8 show the reconstructed density when the Saunders selection function was used. Although our selection function is steeper than that of Saunders (see previous section), the influence on the reconstructed density is not strong. The position of the structures is unaffected, but the fluctuations are slightly larger if the Saunders selection function is used.

In the centres of some voids the reconstruction yields negative densities (overdensities $\delta < -1$). This is due to the fact that the expansion of the density uses only a finite number of modes. As we know that this is not physical but due to the truncation of the expansion series we have set all negative densities to zero.

Figure 4.9 illustrates the statistical errors on the overdensity ($\Delta\delta = \Delta\rho / \langle \rho \rangle$). Light grey dots mark areas with errors between 0.01 and 0.02, black dots between 0.02 and 0.03, crosses between 0.03 and 0.04 and black squares errors of more than 0.04. As one might expect, the errors trace regions with little information, that is behind the mask and at large distances. At large distances the effect of the selection function becomes even stronger than the effect of the angular mask. These errors are statistical errors, and owing to the large number of galaxies in the catalogue they are relatively small. However, in addition there will be systematic uncertainties due to the uncertainties in the selection function. To estimate these requires an investigation with Monte-Carlo simulations.

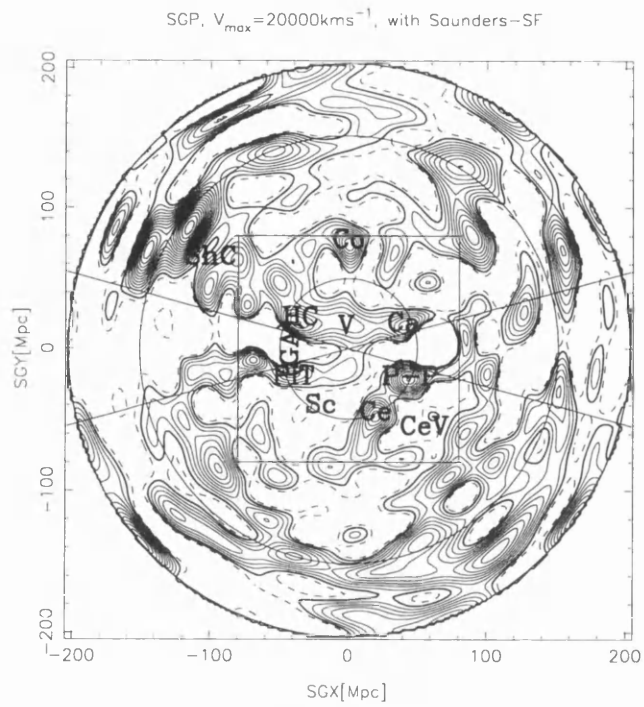


(a) Density field in SGP

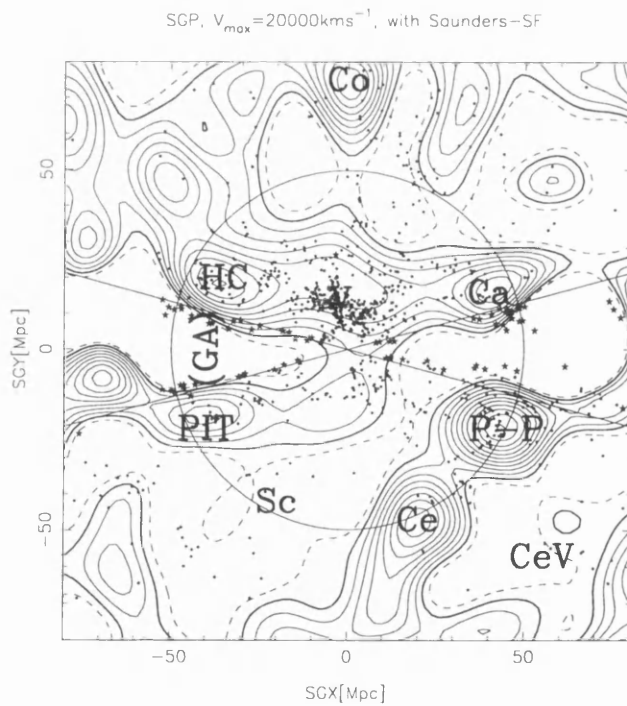


(b) Density field in SGP; clipping from previous figure

Figure 4.6: Same as figure 4.3, but reconstructed with $V_{max} = 25,000 \text{ km s}^{-1}$.

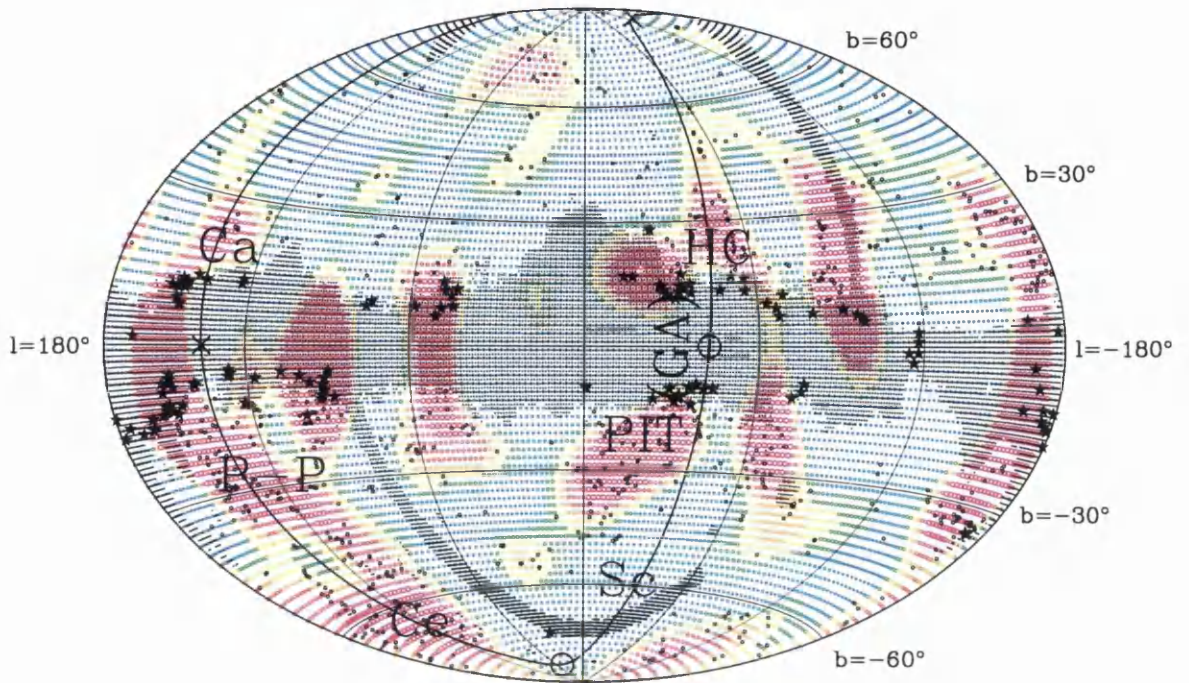


(a) Density field in SGP, reconstructed with Saunders-SF

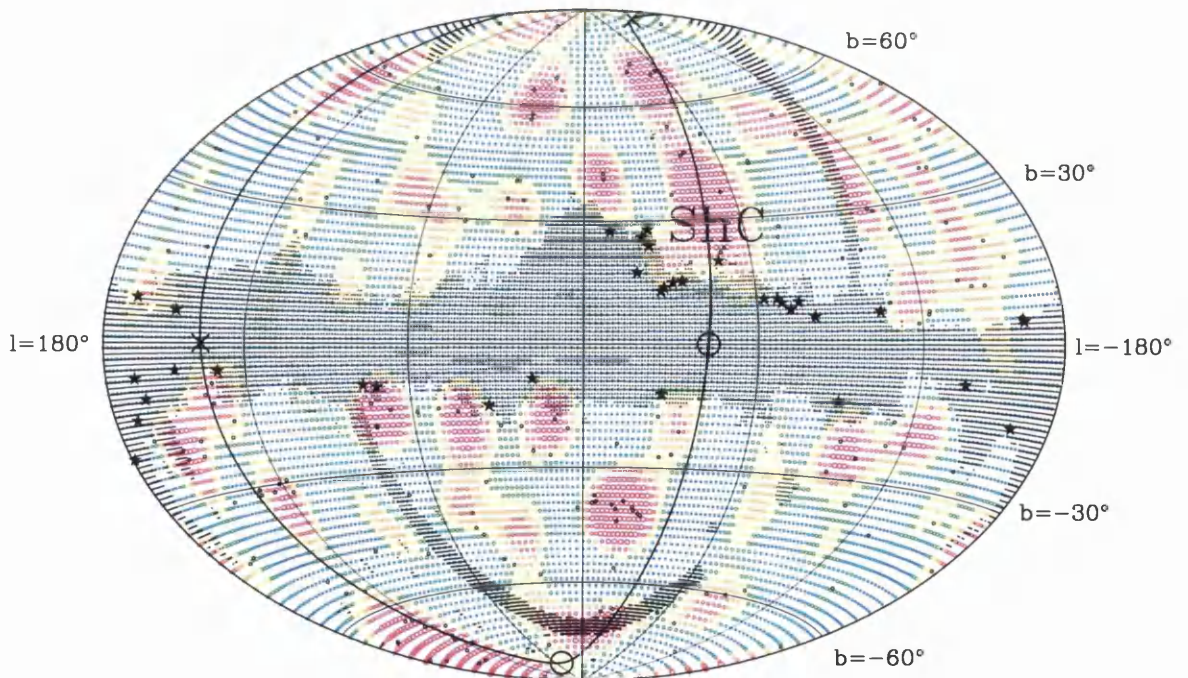


(b) Density field in SGP; reconstructed with Saunders-SF, clipping from previous figure

Figure 4.7: Same as figure 4.3, but reconstructed with Saunders-selection function.

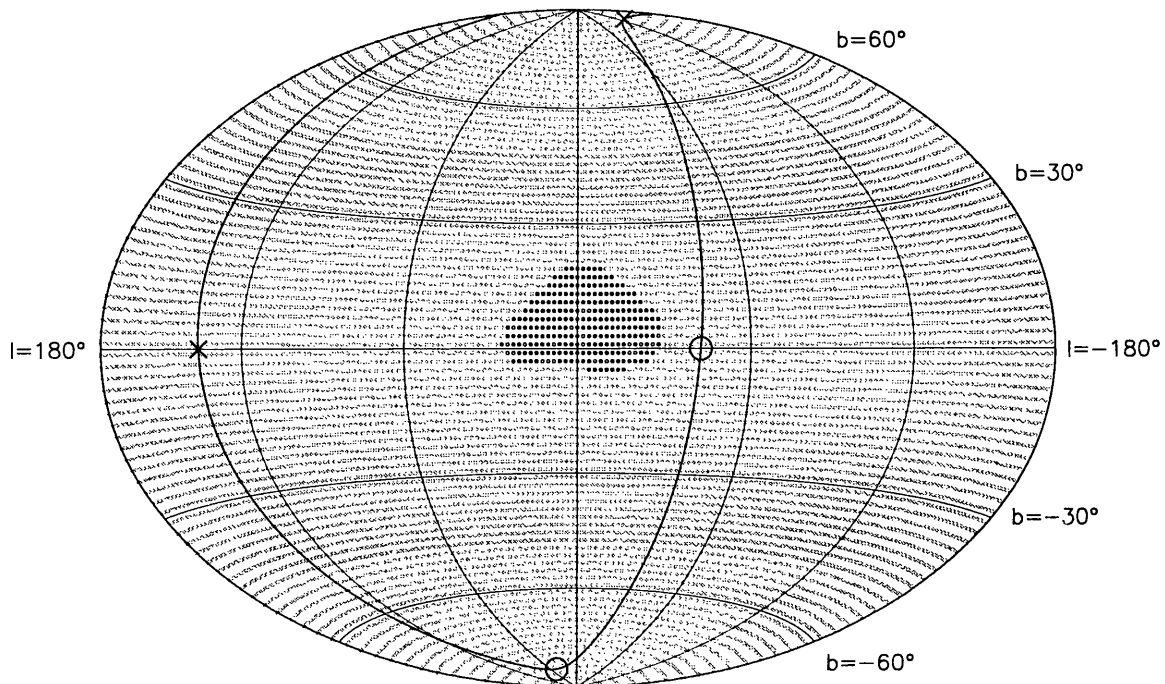


(a) Density in shell $r = 50\text{Mpc}$; with Saunders-SF

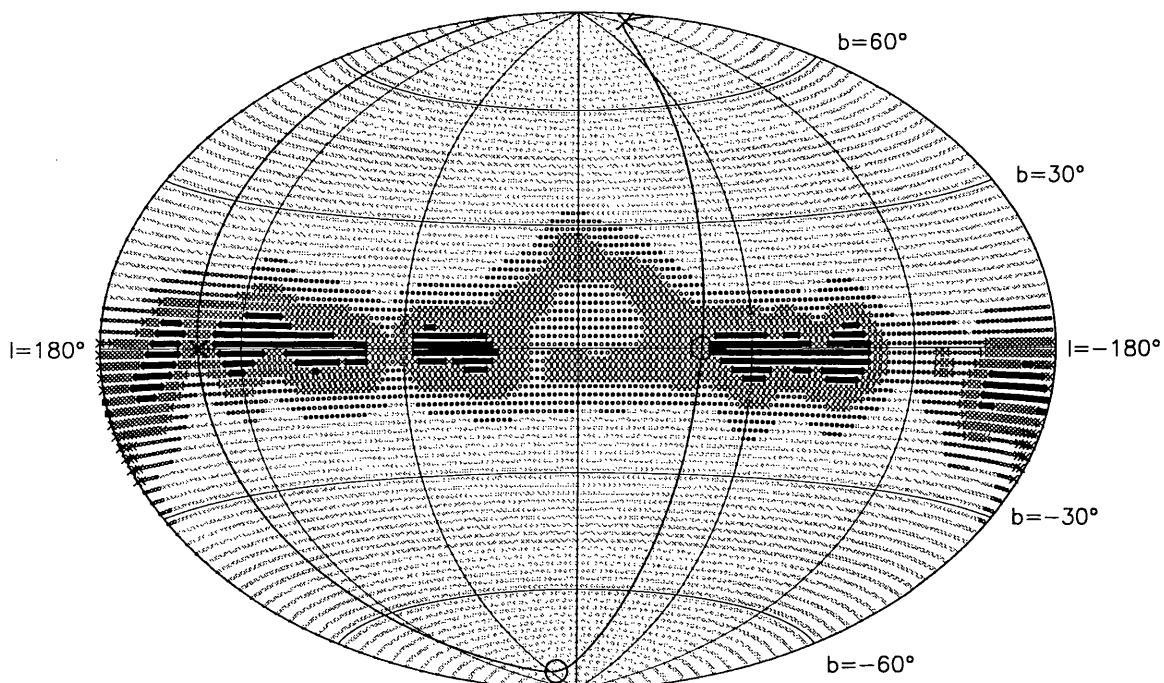


(b) Density in shell $r = 150\text{Mpc}$; with Saunders-SF

Figure 4.8: Same as in figure 4.4, but reconstructed with Saunders-SF.



(a) Errors in the overdensity field in shell $r = 30\text{Mpc}$



(b) Errors in the overdensity field in shell $r = 50\text{Mpc}$

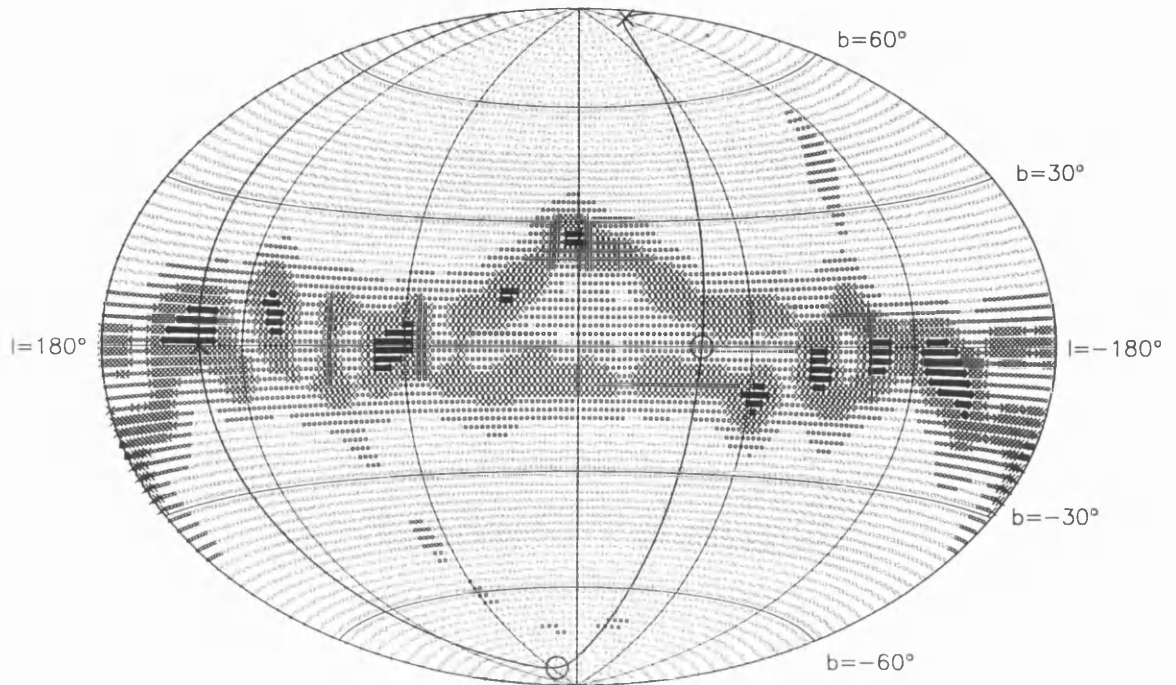
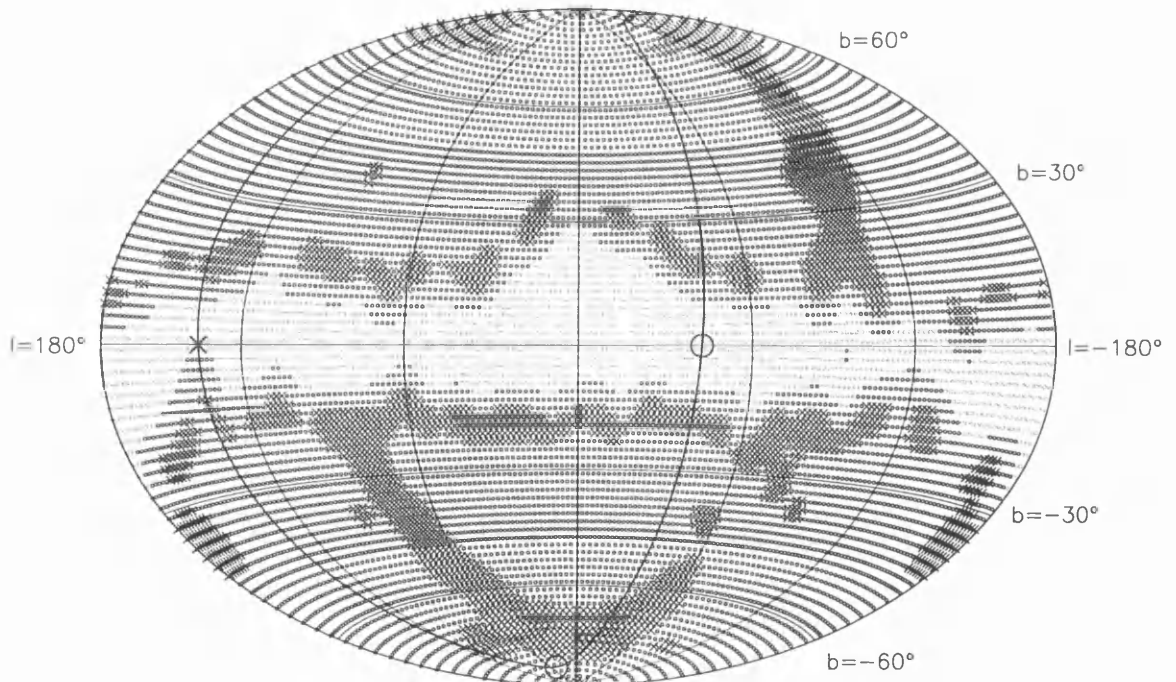
(c) Errors in the overdensity field in shell $r = 70\text{Mpc}$ (d) Errors in the overdensity field in shell $r = 150\text{Mpc}$

Figure 4.9: Errors in the reconstructed density fields, related to the mean density, see text.

Chapter 5

Conclusions

We have presented an alternative method to account for the angular mask and the selection function of redshift catalogues, and applied it to reconstruct the galaxy density from the PSCz catalogue.

At first we construct the selection function for the PSCz catalogue with a robust, non-parametric method. We assume a universal luminosity function, but we make no assumptions about the spatial distribution, and, as the method is non-parametric, we do not assume a certain shape for the luminosity or selection functions. An error analysis on mock catalogues yields a relative error in the selection function of 14%. The selection function is determined up to a normalising constant, but for the reconstruction of the overdensity field this unknown constant cancels out.

The method for the density reconstruction is a variation on the usual expansion of the density field in a set of orthonormal basis functions, adapted to the presence of the selection function and an angular mask. The usual sets of basis functions are orthonormal on the “full space”, but not in the presence of the mask and the selection function (the masked space). The selection function is treated as a radial mask. Therefore, a new set of basis functions that are orthonormal on the masked space is constructed. The new functions are linear combinations of the usual set. They “span” the unmasked space and so are not confused by the lack of information in the masked regions. The density field is then expanded in the new set of functions, whose expansion coefficients can in principle be computed by integrating over the masked space over the functions, respectively. These integrals can be approximated by sums over the galaxies.

We applied the method to the usually orthonormal Spherical Harmonics and Spherical Bessel Functions. The procedure involves the inversion of a large matrix, we used a truncated

Singular Value Inversion to stabilise the inversion. When we reconstructed the density field we also applied a linear regularisation to account for the shot noise. The prior assumption for the regularisation was that the density field is not too different from a constant. Here the use of the new set of functions is an advantage as the covariance matrix is diagonal because of the orthonormality on the masked space. The reconstruction was performed in redshift space.

We tested the influence of a change in the maximum included distance and in the truncation of the expansion and found the result not sensitive to these parameters. We also reconstructed the overdensity field with the Saunders selection function. The positions of the reconstructed structures are hardly affected by the change in the selection function, but the amplitude of the fluctuations is slightly increased.

In regions outside the mask we find our result consistent with the data and with other recent results. As expected the method cannot give reliable results behind the mask, because no information is provided about these regions.

5.1 Future Work

There are several interesting directions in which this research could be extended.

So far we have only investigated the statistical errors in the reconstructed density field, which turned out to be small thanks to the large number of galaxies in the PSCz catalogue. In addition to this there is a systematic error due to the uncertainties in the selection function. The size of this error could be estimated by a Monte-Carlo simulation: the density would be reconstructed for a sufficiently large number of realisations of the selection function, which are generated from the reconstructed selection function and its uncertainties. Indeed, one could also generate an ensemble of mock PSCz catalogues via Monte-Carlo simulations, randomly sampling from both the LF (with errors) and the spatial distribution, and thus determine a reconstructed selection function and density field from each simulation.

Also, the influence of a more sophisticated a priori assumption for the expected density field for the linear regularisation could be investigated.

5.1.1 Going to Real Space

A next step is to go from redshift space to real space. The real space to redshift space distortion only affects the radial coordinate, and it causes mode mixing. As the SH&SB can be separated into angular and radial parts, only the radial modes get mixed, that means

only modes with the same l, m indices. [Fisher et al. 1995] constructed a matrix Z (their eqn. (D17)) so that this mode mixing can be written as

$$\delta_{lmn}^S = \sum_{n'} (Z_l)_{nn'} \delta_{lmn'}^R, \quad (5.1)$$

where $\delta_{lmn'}^R$ are the overdensity coefficients in real space and δ_{lmn}^S the coefficients in redshift space. They included in their coupling matrix also the effect of the selection function which introduces uncertainties in the matrix and makes a direct inversion unstable. For this reason [Fisher et al. 1995] apply a Wiener Filter for the inversion. We have already taken the selection function into account in the coefficients of the overdensity field in redshift space, and so the matrices $(Z_l)_{nn'}$ can be computed without uncertainties, all errors are “attached” to the coefficients δ_{lmn}^S . A direct inversion of equation 5.1 is possible. Along with the conversion to real space the velocity and potential field can be constructed, because in the linear regime the velocity field is the gradient of a potential field, which is related to the density by the Poisson equation. How these relations between the fields translate into relations between their expansion coefficients is explained in e.g. [Fisher et al. 1995].

An alternative method is to convert the redshift density field to the real space field by iteratively solving the system of equations (as e.g. in [Teodoro 1999])

$$\vec{v}(\vec{r}) = \frac{H_0 \beta}{4\pi} \int \frac{\vec{r}' - \vec{r}}{|\vec{r}' - \vec{r}|^3} \delta(\vec{r}') d^3 r' \quad (5.2)$$

$$H_0 \vec{r} = cz - \hat{r}[\vec{v}(\vec{r}) - \vec{v}_{LG}], \quad (5.3)$$

where $\vec{v}(\vec{r})$ is the peculiar velocity at the position \vec{r} , \vec{v}_{LG} the peculiar velocity of the local group, while β is the redshift space distortion parameter $\beta = \Omega^{0.6}/b$ and b the bias parameter.

5.1.2 Power Spectrum Estimation

After the method is extended to real space it provides a tool to estimate the power spectrum of the density fluctuations. This is an important task because the power spectrum contains information about the initial fluctuations in the mass density as well as the evolution of these fluctuations. Theories like inflation predict a primordial power spectrum which is often of a power law form

$$P(k) = Ak^n, \quad (5.4)$$

where n is called the spectral index. The initial power spectrum is then “processed” by the growth of structure. How this evolution proceeds depends on parameters like the Hubble Constant H_0 , and the density parameter $\Omega_0 = \rho_0/\rho_{crit}$ which is just the ratio of the mean

density ρ_0 and the critical density ρ_{crit} that would be needed to give our universe a flat geometry. Also the cosmological constant Λ and the kind of dark matter (cold dark matter, hot dark matter, a mixture of both, ...) have a strong impact. This change in the shape of the power spectrum is summarised in the transfer function $T(k, t)$, so that the initial power spectrum is related to the evolved one by

$$P(k, t_0) = \left[\frac{b(t_0)}{b(t_i)} \right]^2 T(k, t_0) P(k, t_i), \quad (5.5)$$

where t_i is the initial time and t_0 is the time of the observation. The function $b(t)$ describes the linear growth of perturbations above the Jeans scale, it is the law that we investigated in the introduction. If this growth of perturbations were the only effect on the power spectrum, it would be just rescaled.

One now can assume an initial power spectrum and derive a transfer function from numerical simulations for different assumed cosmological models, and predict the power spectrum we observe today. Here also a model for how galaxies trace the underlying mass density (bias) needs to be incorporated, as we can only observe the luminous matter.

A comparison to the actual data can put constraints on the parameters that characterise the model or can perhaps reject some the models completely. Of course the power of the constraints depends on the accuracy of the measured power spectrum.

I hope that the method developed in this thesis will be a further step on the way to discover ...

“... was die Welt
im Innersten zusammenhält.”
 (“... whatever holds
the world together in its inmost folds.”)

J.W. Goethe, *Faust: Der Tragödie erster Teil*, 1808

References

- [Binney and Tremaine 1987] Binney J., Tremaine S., 1987, *Princeton Series in Astrophysics* (Galactic Dynamics)
- [Coles and Lucchin 1995] Coles P., Lucchin F., 1995, *John Wiley & Sons Ltd.* (Cosmology: The Origin and Evolution of Cosmic Structure)
- [Coles 1997] Coles P., 1997, *ASP Conference Series*, Vol.126, Chapter 9 (p. 233-278)
- [Fisher et al. 1995] Fisher K.B., Lahav O., Hoffman Y., Lynden-Bell D., Zaroubi S., 1995, *MNRAS* 272:885
- [Gorski 1994] Gorski K.M., 1994, *ApJ* 430:L85
- [Heavens and Taylor 1995] Heavens A.F., Taylor A.N., 1995, *MNRAS* 275:483
- [Humason et al. 1956, appendix B] Humason M.L., Mayall N.U., Sandage A., 1956, *Astron. J.* 61:97
- [Lahav et al. 1994] Lahav O., Fisher K.B., Hoffman Y., Scharf C.A., Zaroubi S., 1994, *ApJ* 423:L93
- [Lawrence et al. 1999] Lawrence A., Rowan-Robinson M., Ellis R. S., Frenk C. S., Efstathiou G., Kaiser N., Saunders W., Parry I. R., Xiaoyang Xia, Crawford J., 1999, *MNRAS* 308:L897
- [Lynden-Bell 1971] Lynden-Bell D., 1971, *MNRAS* 155:95
- [Lynden-Bell et al. 1989] Lynden-Bell D., Lahav O., Burstein D., 1989, *MNRAS* 241:325
- [Peacock 1999] Peacock J.A., 1999, *Cambridge University Press* (Cosmological Physics)
- [Press et al. 1992] Press, W.H., Teukolsky S.A., Vetterling W.T., Flannery B.P., 1992, *Cambridge University Press* (Numerical Recipes)

- [Rauzy and Hendry 2000] Rauzy S., Hendry M.A., 2000, *MNRAS* in press
- [Saunders et al. 1990] Saunders W., Rowan-Robinson M., Lawrence A., Efstathiou G., Kaiser N., Ellis R.S., Frenk C.S., 1990, *MNRAS* 242:318
- [Saunders et al. 2000] Saunders W., Sutherland W.J., Maddox S.J., Keeble O., Oliver S.J., Rowan-Robinson M., McMahon R.G., Efstathiou G.P., Tadros H., White S.D.M., Frenk C.S., Carramiñana A., Hawkins M.R.S., 2000, *MNRAS*, submitted
- [Schechter 1976] Schechter P., 1976, *ApJ* 203:297
- [Schmidt 1968] Schmidt M., 1968, *ApJ* 151:393
- [Springel and White 1998] Springel V., White S.D.M., 1998, *MNRAS* 298:143
- [Strauss and Willick 1995] Strauss M.A., Willick J.A., 1995, *Phys. Reports* 261:271
- [Tadros et al. 1999] Tadros H., Ballinger W.E., Taylor A.N., Heavens A.F., Efstathiou G., Saunders W., Frenk C.S., Keeble O., McMahon R., Maddox S.J., Oliver S., Rowan-Robinson M., Sutherland W.J., White S.D.M., 1999, *MNRAS* 305:527
- [Teodoro 1999] Teodoro L.F.A., 1999, PhD-Thesis
- [Yahil et al. 1977] Yahil A., Tammann G.A., Sandage A., 1977, *ApJ* 217:903
- [Yahil et al. 1991] Yahil A., Strauss M.A., Davis M., Huchra J.P., 1991, *ApJ* 372:380
- [Zaroubi et al. 1995] Zaroubi S., Hoffman Y., Fisher K.B., Lahav O., 1995, *ApJ* 449:446

